



**HAL**  
open science

## **The histone variant macroH2A1.1 regulates gene expression by direct association with their transcription start site**

Ludmila Recoules, Alexandre Heurteau, Flavien Raynal, Fatima Moutahir, Fabienne Bejjani, Isabelle Jariel-Encontre, Olivier Cuvier, Anne-Claire Lavigne, Kerstin Bystricky

### ► To cite this version:

Ludmila Recoules, Alexandre Heurteau, Flavien Raynal, Fatima Moutahir, Fabienne Bejjani, et al.. The histone variant macroH2A1.1 regulates gene expression by direct association with their transcription start site. 2020. <hal-03037462>

**HAL Id: hal-03037462**

**<https://hal.science/hal-03037462v1>**

Preprint submitted on 3 Dec 2020

HAL is a multi-disciplinary open access archive for the deposit and dissemination of scientific research documents, whether they are published or not. The documents may come from teaching and research institutions in France or abroad, or from public or private research centers.

L'archive ouverte pluridisciplinaire HAL, est destinée au dépôt et à la diffusion de documents scientifiques de niveau recherche, publiés ou non, émanant des établissements d'enseignement et de recherche français ou étrangers, des laboratoires publics ou privés.



HAL Authorization

1  
2  
3  
4  
5  
6  
7  
8  
9  
10  
11  
12  
13  
14  
15  
16  
17  
18  
19  
20  
21  
22  
23  
24

**The histone variant macroH2A1.1 regulates gene expression by direct association with their transcription start site.**

Ludmila Recoules<sup>1</sup>, Alexandre Heurteau<sup>1</sup>, Flavien Raynal<sup>1</sup>, Fatima Moutahir<sup>1</sup>,  
Fabienne Bejjani<sup>3</sup>, Isabelle Jariel-Encontre<sup>3</sup>, Olivier Cuvier<sup>1</sup>, Anne-Claire Lavigne<sup>1\*</sup>  
and Kerstin Bystricky<sup>1,2\*</sup>.

<sup>1</sup> Laboratoire de Biologie Moléculaire Eucaryote (LBME), Centre de Biologie Intégrative (CBI), Université de Toulouse, CNRS, UPS, F-31062 Toulouse, France.

<sup>2</sup> Institut Universitaire de France (IUF).

<sup>3</sup> Institut de Génétique Moléculaire de Montpellier, CNRS, UMR5535, Equipe Labellisée Ligue Nationale contre le Cancer, F-34293, France.

\*Corresponding authors.

E-mails : [kerstin.bystricky@ibcg.biotoul.fr](mailto:kerstin.bystricky@ibcg.biotoul.fr) ; [anne-claire.lavigne@ibcg.biotoul.fr](mailto:anne-claire.lavigne@ibcg.biotoul.fr)

## 25 **Abstract**

26       The histone variant macroH2A1 (mH2A1) is involved in cellular growth,  
27 differentiation and reprogramming, but the underlying molecular mechanisms are a  
28 matter of debate. Different roles of mH2A1 in gene expression may relate to  
29 functional differences of its two splicing isoforms, mH2A1.1 and mH2A1.2. Here, we  
30 map for the first time genome-wide localization of endogenous mH2A1.1 and link the  
31 distribution of mH2A1.1 to control of gene expression in human breast cancer cells.  
32 In addition to localization shared with mH2A1.2 to facultative heterochromatin,  
33 mH2A1.1 specifically associates with regulatory elements required for gene  
34 activation, super-enhancers and promoters of highly expressed genes. Depending on  
35 the recruitment profile of mH2A1.1 to these elements, selective depletion of mH2A1.1  
36 up- or downregulates its target genes. mH2A1.1 represses transcription when its  
37 binding is spread over the entire gene and promoter, and activates transcription  
38 when its binding is strictly confined to the transcription start site (TSS). Notably, RNA  
39 Polymerase II was frequently in pause at mH2A1.1-activated genes. Functionally,  
40 mH2A1.1-dependent regulation of a subset of paused genes impedes mammary  
41 tumor cell migration. Molecular mechanisms of mH2A1.1 function at the TSS  
42 uncovered by our study define an intriguing new mode of transcription regulation in  
43 cancer cells.

44

## 45 **Author Summary**

46

47       Control of gene expression driving cellular functions from differentiation to  
48 epistasis and causing, when dysfunctional, uncountable diseases, relies on  
49 modifications of chromatin structure. One key element enabling chromatin plasticity is

50 the replacement of canonical histones by histone variants. Among histone variants  
51 macroH2A1 (mH2A) is an extraordinary H2A variant possessing a large non-histone  
52 domain placed outside of the nucleosome. Two splicing isoforms, mH2A1.1 and  
53 mH2A1.2, are produced, but these are rarely studied separately because they only  
54 differ in a 30 amino acid region and are difficult to distinguish experimentally, which  
55 likely explains contradictory functions reported in the literature. Here, we take  
56 advantage of a mH2A1.1 specific antibody to generate the first genome-wide  
57 chromatin-associated map of this histone variant in the invasive breast cancer cells  
58 line MDA-MB231. We confirm that mH2A1.1, like mH2A1.2, is enriched at facultative  
59 heterochromatin in agreement with its reported role as a repressor. However, we  
60 discovered that unlike its splicing isoform, mH2A1.1 specifically binds to super-  
61 enhancers and the transcription start site of highly transcribed genes. mH2A1.1 is  
62 necessary for regulating transcription of these genes. At the cellular level, we  
63 demonstrate that mH2A1.1 inhibits migration capacity of highly metastatic breast  
64 cancer cells. Our study characterizes for the first time binding profiles of mH2A1.1  
65 that are linked to regulation of gene expression, thereby providing a new molecular  
66 mechanisms which govern the plasticity of human tumor cells.

67

## 68 **Introduction**

69 Compaction of DNA into chromatin modulates DNA accessibility, thereby  
70 regulating key molecular processes such as transcription [1,2]. Histone post-  
71 translational modifications, chromatin-remodeling enzymes, DNA-binding factors and  
72 architectural proteins fine-tune genome organization and dynamics [1,2]. In addition,  
73 histone variants replace canonical histones in a locus-specific manner, which endows

74 chromatin with additional properties required to regulate DNA accessibility and  
75 functions [3].

76         Among the histone variants, macroH2A1 (mH2A1) is a vertebrate-specific [4,5]  
77 histone H2A variant composed of an N-terminal H2A-like domain (64 % identical to  
78 H2A) and a C-terminal 25 kDa ‘macro’ domain. These two domains are joined by an  
79 unstructured 41 amino acid long linker that positions the macro domain outside of the  
80 nucleosome [6]. Expression of the highly conserved *H2AFY* gene produces two  
81 splicing isoforms, mH2A1.1 and mH2A1.2, whose sequences differ in a 30 amino-  
82 acid region within the macro domain [6].

83         mH2A1 was originally found to be enriched on the transcriptionally silent X  
84 chromosome [7]. mH2A1 is also present at autosomes, forming large domains in  
85 association with histone marks associated with heterochromatin, such as H3K27me3  
86 and H3K9me3 [8–10]. *In vitro* studies have demonstrated that nucleosomal mH2A1  
87 interferes with binding of the transcription factor NFκB, and inhibits nucleosome  
88 sliding by the remodeling complex SWI/SNF and initiation of RNA polymerase II (Pol  
89 II) transcription [11,12]. Therefore, mH2A1 is believed to play a role in transcriptional  
90 repression. However, in a few cases the presence of mH2A1 has been seen to  
91 correlate with active transcription of a subset of genes involved in a variety of  
92 processes such as cell differentiation, lipid metabolism and cell-cell signaling [8,13–  
93 17]. Thus, the roles of mH2A1 in regulating gene expression are seemingly  
94 contradictory. Studying mH2A1 isoforms separately may help to better understand  
95 their roles.

96         The two mH2A1 splice variants exhibit tissue- and cell-specific expression  
97 patterns[18]. In normal cells, the mH2A1.2 isoform appears ubiquitously expressed  
98 [19–21]. Mainly incorporated into heterochromatin (X-inactive chromosome and

99 autosomic heterochromatin) [7–9,22], this splicing isoform is generally associated  
100 with gene repression. However, a few recent studies discovered that mH2A1.2 was  
101 required for gene expression. Indeed, in mouse muscle cells [13], mH2A1.2 binds  
102 muscle-specific enhancers necessary for the activation of the myogenic regulator  
103 network. In human embryonic stem cells (hESCs) [23], binding of mH2A1.2 to gene  
104 promoters seems to control gene expression both positively and negatively.  
105 However, the binding profile of mH2A1.2 in hESC was not conserved in mesoderm-  
106 derived human fibroblasts [23].

107 In contrast to mH2A1.2, mH2A1.1 is only expressed in differentiated cells with  
108 low proliferation rates [19–21]. In tumors, expression of the mH2A1.1 isoform is  
109 frequently reduced, as compared to normal tissues, suggesting that this isoform is a  
110 tumor suppressor [20,21,24]. In highly metastatic cancers such as triple-negative  
111 breast cancers however, expression levels of mH2A1.1 are increased and correlate  
112 with poor prognosis [24].

113 Only mH2A1.1 can bind NAD<sup>+</sup> metabolites through its macro domain [25] and  
114 interact with the DNA-damage repair and chromatin remodeling factor PARP1 (Poly-  
115 (ADP-Ribose) Polymerase 1) [14,26–28]. Interaction between mH2A1.1 and PARP1  
116 seems to be key for the capacity of mH2A1.1 to regulate DNA damage responses  
117 [29,30], mitochondrial respiration [28] and gene transcription [14,27,31]. In particular,  
118 it was proposed that mH2A1.1 and PARP1 recruit CBP (CREB-binding protein) to  
119 mediate acetylation of H2BK12/K120 and to regulate, in part, mH2A1-target gene  
120 expression in IMR90 cells, without really demonstrated the specific action of  
121 mH2A1.1 with respect to mH2A1.2 [14]. In other hand, recruitment of mH2A1.1 to  
122 repressed signal-inducible genes is required for their stress response [31,32].  
123 Despite this knowledge about functions of mH2A1.1, neither its chromatin

124 association, independently of the one of mH2A1.2, nor its specific mechanisms of  
125 action during gene activation, was clearly analyzed.

126 To gain a better understanding of the roles of mH2A1.1 in regulating gene  
127 expression, we determined 1) the genomic localization of mH2A1.1 and 2) its effect  
128 on gene expression. To that end, we generated a ChIP-grade mH2A1.1-specific  
129 antibody. Chromatin immunoprecipitation followed by sequencing (ChIP-seq) of  
130 mH2A1.1, of total mH2A1 and of a variety of histone marks, shows that both mH2A1  
131 isoforms bind to heterochromatin and to enhancers. Surprisingly, only the mH2A1.1  
132 isoform binds TSSs (Transcription Start Site) of active genes. Interestingly, we show  
133 that mH2A1.1-activated genes are mostly Pol II paused genes. Frequently, these  
134 genes are negatively implied in cell migration in mammary tumor cells. We  
135 demonstrate that mH2A1.1 impedes cell migration whereas mH2A1.2 promotes it.  
136 Our work describes a novel gene activation pathway in cancer cells dependent on  
137 the selective recruitment of mH2A1.1 to the TSS of paused genes.

138

## 139 **Results**

140

141 **mH2A1.1 and mH2A1.2 preferentially associate with facultative**  
142 **heterochromatin.** We determined the genomic localization of mH2A1.1 in the  
143 claudin-low breast cancer cell line MDA-MB231 which expresses this histone variant  
144 at a high level compared to other types of breast cancer cell lines (S1A, S1B Fig)  
145 [24]. To that end, we developed a ChIP-grade polyclonal rabbit antibody that  
146 exclusively recognizes mH2A1.1 (Ab  $\alpha$ mH2A1.1) (S1C-S1F Fig) By ChIP-seq, we  
147 determined the distribution of mH2A1.1 and of total mH2A1 using Ab  $\alpha$ mH2A1.1 and

148 a commercially available ChIP-grade antibody (Ab37264 (Ab  $\alpha$ mH2A1)) (S1, S2  
149 Tables and S1G-S1I Fig), respectively.

150 We identified 29,112 peaks for mH2A1.1 (Ab  $\alpha$ mH2A1.1) and 22,789 peaks for  
151 total mH2A1 (Ab  $\alpha$ mH2A1), covering combined 13.6 % of the genome. Genome-  
152 wide, ChIP-seq results obtained with these two antibodies were highly similar with a  
153 significant co-occurrence of peaks (Fisher exact test (FET): p-value  $< 2.2 \times 10^{-16}$  and  
154 Odd ratio = 27.40) and a Pearson coefficient correlation (PCC) of 0.92 (S2A Fig).

155 Analysis of peaks detected with Ab  $\alpha$ mH2A1 and Ab  $\alpha$ mH2A1.1 shows that  
156 regions occupied by mH2A1.1 and mH2A1.2 do not overlap completely (Fig 1A)  
157 suggesting that some regions are preferentially bound by either one of the variants.  
158 Indeed, a significant number of sites (18,838) is preferentially recognized by Ab  
159  $\alpha$ mH2A1.1 and not by Ab  $\alpha$ mH2A1 (Fig 1A). Of note, Ab  $\alpha$ mH2A1 has lower efficacy  
160 than Ab  $\alpha$ mH2A1.1 in detecting mH2A1.1 and may, when reducing detection  
161 thresholds, recognize a fraction of these sites (S1B, S1G, S1H Fig). Genomic regions  
162 common to both antibodies correspond to one or more peaks exclusively recognized  
163 as mH2A1.1 or both isoforms in unknown relative proportions. For further analysis,  
164 we defined three types of genomic regions: regions incorporating preferentially only  
165 mH2A1.1 (mH2A1.1 only), regions incorporating preferentially only mH2A1.2  
166 (mH2A1.2 only) and regions incorporating either mH2A1.1 or both isoforms  
167 (mH2A1s) (Fig 1A).

168 These ChIP-seq results raise the possibility that preferential genomic  
169 localization of the mH2A1.1 variant relate to its function. To test this possibility, we  
170 first characterized the distribution of mH2A1.1 ChIP-seq peaks with respect to  
171 selected genomic features (Fig 1B; see Materials and Methods). Nearly one third of

172 mH2A1.1 peaks were associated with distal intergenic regions and another third of  
173 mH2A1.1 peaks with promoters (TSS $\pm$ 1kb) (Fig 1B).

174 Next, we analyzed mH2A1.1 genomic localization with respect to the  
175 chromatin environment of the identified regions. We first integrated ENCODE ChIP-  
176 seq of heterochromatin histone marks (H3K9me3 and H3K27me3) [33]. We found  
177 that genome-wide, mH2A1.1 ChIP-seq peaks were significantly enriched with the  
178 H3K27me3 repressive histone mark, in a manner comparable to the one observed  
179 using Ab  $\alpha$ mH2A1 (Figs 1C and S2A). We confirmed the enrichment of mH2A1.1 on  
180 heterochromatin domains in independent ChIP-qPCR experiments on WT and  
181 mH2A1.1-deficient cells using two different siRNAs directed against mH2A1.1  
182 isoform (S3A-S3E and S4 Figs). Remarkably, even if the related PCCs were low  
183 between H3K9me3 and mH2A1 isoforms (S2A Fig), in particular for mH2A1.1, we  
184 detected that both mH2A1 isoforms overlapped significantly with H3K9me3 (Fig 1C).  
185 At heterochromatin domains (i.e. marked by H3K27me3 and/or H3K9me3), both  
186 mH2A1 ChIP-seq peaks were highly similar with a PCC of 0.94 (S2B Fig).  
187 Surprisingly, 80% of H3K27me3 overlapped with H3K9me3 (Fig 1C), although often  
188 presented as non-overlapping heterochromatin histone marks [34]. However, within  
189 peaks common to H3K27me3 and H3K9me3, the contribution of each mark was  
190 inversely proportional (Figs 1D and S5A). In addition, a high H3K27me3 to H3K9me3  
191 ratio was more associated with genes whereas low H3K27me3 to H3K9me3 ratio  
192 was more associated with gene-poor genomic regions (Fig 1D and S5B). Hence, in  
193 this cell line, levels of relative enrichment between H3K27me3 and H3K9me3 could  
194 be used to distinguish “facultative-like” heterochromatin (with high levels of  
195 H3K27me3 and low levels of H3K9me3), from “constitutive-like” heterochromatin  
196 (with low levels of H3K27me3 and high levels of H3K9me3). In this context, we

197 observed that the genomic distribution of both mH2A1 isoforms positively correlates  
198 with regions rich in H3K27me3 and poor in H3K9me3 levels, hence corresponding to  
199 “facultative-like” heterochromatin (Fig 1E).

200

201 **mH2A1.1 binds to super-enhancers.** Because a large number of mH2A1.1 sites  
202 are associated with promoter regions (Fig 1B), we performed ChIP-seq experiments  
203 for a panoply of histone marks usually associated with active transcription  
204 (H3K4me1, H3K4me3, H3K27ac and H3K36me3) (*Bejjani et al, in preparation*). We  
205 found that mH2A1.1 correlated positively with H3K4me1 and H3K27ac, two  
206 chromatin modifications which characterize active enhancer regions [35] (Figs 2A  
207 and S2A). We found that more than 40% of mH2A1.1 and total mH2A1 overlapped  
208 significantly with “putative” enhancers outside of TSSs (Fig 2B; see Materials and  
209 Methods). 17% of “putative” enhancers were bound by mH2A1 isoforms. Among  
210 them, some were common to mH2A1.1 and total mH2A1 (48%) but many were only  
211 bound by mH2A1.1 (33%) or by mH2A1.2 (19%). At “putative” enhancers, both  
212 mH2A1 ChIP-seq results were still similar with a PCC of 0.80 (S2B Fig). Interestingly,  
213 mH2A1-bound regions frequently formed large domains comprising a group of  
214 enhancers marked with H3K27ac (Fig 2C), which could correspond to super-  
215 enhancers (SE) [36,37]. Using the ROSE package to detect SEs marked by the  
216 H3K27ac signal [36,37], we identified “putative” SEs in MDA-MB231 cells (Materials  
217 and Methods). We show that 85% of these SEs were bound by at least one mH2A1  
218 isoform, 19% of them were associated with mH2A1.1 compared to only 3% with  
219 mH2A1.2 only (Fig 2D). The enrichment of mH2A1.1 at super-enhancers was  
220 confirmed in independent ChIP-qPCR experiments in WT and mH2A1.1-deficient

221 cells using two different siRNAs directed against the mH2A1.1 isoform (S3A-S3E and  
222 S4 Figs).

223

224 **mH2A1.1 binds to the transcription start site of active genes.** A striking genomic  
225 feature identified for mH2A1.1 was its binding to TSSs (+/- 1kb) (hereafter referred to  
226 as “promoter regions”) (Fig 1B) confirmed by independent ChIP-qPCR experiments  
227 in WT and mH2A1.1-deficient cells by two different siRNAs directed against  
228 mH2A1.1 isoform (S3A-S3E and S4 Figs). Therefore, we characterized the  
229 association of mH2A1 isoforms at these genomic sites in more detail. Our ChIP-seq  
230 data showed that mH2A1.1 was more frequently associated with promoter regions  
231 than mH2A1 (41% vs 35%, respectively) (Fig 3A). Interestingly, among promoter  
232 regions bound by mH2A1 isoforms, 45% of them were occupied by mH2A1.1 only,  
233 whereas 14% were occupied by mH2A1.2 only (Fig 3A). We thus wondered whether  
234 the chromatin environment of promoter regions correlates with specific binding of  
235 either isoform. At promoter regions, we found that mH2A1.1 positively correlated with  
236 active marks (H3K4me3 and Pol II) whereas mH2A1 positively correlated with  
237 repressive histone marks (H3K27me3 and H3K9me3) (S6A Fig). Interestingly, this  
238 difference in localization identified by the two antibodies was maintained when we  
239 considered the two genomic populations specific to each antibody, mH2A1.1 only  
240 and mH2A1.2 only (S6B, S6C Fig). These results strongly suggest that mH2A1.2  
241 preferentially binds to promoters in a closed chromatin state whereas mH2A1.1 is  
242 mainly recruited to promoters in an open chromatin state. In agreement, at promoter  
243 regions, both mH2A1 ChIP-seq experiments differed from one another with a PCC of  
244 0.41 (in comparison to a PCC of 0.92 genome-wide) (S2A, S2B Fig). To assess  
245 whether mH2A1.1 binding at the TSS correlates with transcription levels, we

246 generated RNA-seq data from MDA-MB231 cells. We then stratified genes into four  
247 equal categories according to their expression levels (from silent to highly expressed  
248 genes). We determined the distribution of both mH2A1 isoforms at the TSS (+/- 2 kb)  
249 and over the gene body (region from the TSS to the Transcription End Site (TES)) for  
250 those four groups of genes (see Materials and Methods). We found that the amount  
251 of mH2A1.1 bound to TSSs increased with expression levels while relative amounts  
252 recruited onto gene bodies decreased (Figs 3B, 3C and S7A-S7D). On the contrary,  
253 mH2A1 bound uniformly to TSSs and over the gene body of silent genes and its  
254 presence was restricted to the proximal promoter regions (around 1kb upstream  
255 TSSs) and downstream of TESs of expressed genes (Figs 3B, 3C and S7A-S7D). In  
256 agreement, mH2A1.1 peaks were mainly present at the TSS +/- 1kb of highly  
257 transcribed genes (Fig 3D), while mH2A1 peaks were present on the TSSs +/- 1kb of  
258 silent genes (Fig 3D). Similar observations were seen for active and repressive  
259 histone marks (S7E Fig). Here again, this difference in localization identified by the  
260 two antibodies was even stronger when we considered the two genomic populations  
261 specific to each antibody, mH2A1.1 only and mH2A1.2 only (Fig 3D). Notably, we  
262 observed that mH2A1.1 binding at TSSs was distributed uniformly around TSSs,  
263 peaking at maximum Pol II binding (Fig 3E). In agreement, at TSSs, 70% of  
264 mH2A1.1 peaks (two third of them being mH2A1.1 only) overlapped significantly with  
265 Pol II (Fig 3F), with a PCC of 0.48 (in comparison to a PCC of 0.07 genome-wide)  
266 (S2A and S7F Figs). Coherent with these results, mH2A1.2 only peaks were hardly  
267 detectable (3%) at Pol II TSS-bound sites (Fig 3F), and at TSSs, both mH2A1 ChIP-  
268 seq are anti-correlated with a PCC of -0.07 (S2B Fig). These results highlight highly  
269 specific association of the mH2A1.1 variant with the TSSs of transcribed genes.

270

271 **mH2A1.1 regulates gene expression.** Binding of mH2A1.1 to TSSs of transcribed  
272 genes prompted us to test whether mH2A1.1 was required for modulating gene  
273 expression. We generated RNA-seq data from MDA-MB231 cells in which mH2A1.1  
274 protein expression was reduced by around 90 % by siRNA without significantly  
275 affecting expression of the mH2A1.2 isoform (S3A-S3C Fig). 533 genes (56.3%)  
276 were down-regulated (mH2A1.1-activated genes) and 412 genes (43.7%) were up-  
277 regulated (mH2A1.1-repressed genes) in mH2A1.1 knock-down (mH2A1.1 KD)  
278 conditions compared to WT conditions (Fig 4A, S8A and S3 Table). Altered gene  
279 expression was confirmed by RT-qPCR on a subset of genes using two different  
280 siRNAs directed against the mH2A1.1 isoform (S3 Fig). We found that all mH2A1.1  
281 regulated genes, activated- as well as repressed- genes, were active or even highly  
282 expressed genes in WT conditions (S8B and S8C Fig). Strikingly, we revealed that  
283 mH2A1.1 and mH2A1 binding differed between mH2A1.1-activated and repressed  
284 genes (Figs 4B-4D and S9A). Indeed, mH2A1.1 was mainly bound upstream of the  
285 TSS and within the gene body of mH2A1.1-repressed genes. At mH2A1.1-activated  
286 genes, however, mH2A1.1 exclusively associated with the TSSs and upstream (up to  
287 1kb) (Figs 4B-4D and S9A). mH2A1 was bound upstream and downstream of the  
288 TSS of mH2A1.1-repressed genes, whereas its level was at its lowest at the TSS. In  
289 contrast, its relative enrichment was very low at mH2A1.1-activated genes, with its  
290 highest levels upstream TSS (up to 1 kb) (Figs 4B-4D and S9A). Overall, these  
291 results suggest that mH2A1.1 promotes transcription when its binding is restricted to  
292 TSSs and represses transcription when its binding is spread over genes.

293

294 **mH2A1.1 regulates expression of paused genes.** We noted that Pol II was bound  
295 to the TSSs of mH2A1.1-activated genes but was barely detected on the

296 corresponding gene bodies (Figs 4B-4D and S9A). This pattern of Pol II distribution  
297 raised the possibility that mH2A1.1-activated genes may be in pause. To confirm this,  
298 we calculated the Pol II pausing index (PI) for transcribed genes using Pol II ChIP-  
299 seq data as described in [38] (see Materials and Methods). To see if the binding of  
300 mH2A1.1 at TSSs was related to the level of Pol II pausing, we first plotted the  
301 mH2A1.1 ChIP-seq signal around the TSS +/- 10 kb for each gene ranked by their PI  
302 (Fig 5A). We observed that confinement of mH2A1.1 to the TSS and its absence  
303 from the gene body is a characteristic of genes with a high PI. Genes where  
304 mH2A1.1 was spread along the entire gene body were characterized by low PIs (Fig  
305 5A). In agreement, we found that mH2A1.1 peaks, as well as Pol II ones, were  
306 significantly sharper at the TSS (TSS +/- 1kb) of genes with a high PI as opposed to  
307 genes with a low PI (Figs 5B, 5C and S9B). Moreover, 40% of genes bound by  
308 mH2A1.1 only at the TSS have a PI > 2 and 31% of paused genes (defined as genes  
309 with PI>2, n=6,821) have mH2A1.1 only peaks at their TSS (Fig 5D). Furthermore,  
310 the correlation between mH2A1.1 binding and activation of paused genes appeared  
311 to be functionally relevant because the majority of mH2A1.1-activated genes (68%)  
312 have a pausing index greater than 2 and their PI are significantly higher than that of  
313 any other gene category tested (Fig 5E and 5F). In contrast, the majority of  
314 mH2A1.1-repressed genes (69%) was characterized by a PI < 2. These results  
315 suggest that mH2A1.1 spreading over the gene body represses genes whose  
316 expression is independent of Pol II pausing, whereas mH2A1.1 restricted to the TSS  
317 activates genes whose expression is dependent of Pol II pausing. Altogether, our  
318 results provide the first evidence of a functional link between the binding of mH2A1.1  
319 at TSSs and Pol II pausing at promoter proximal regions. We propose that the

320 association of mH2A1.1 with the TSSs of a subset of paused genes enhances their  
321 transcription.

322

323 **mH2A1.1 inhibits cell migration in MDA-MB231 cells.** We found that genes de-  
324 regulated by the loss of mH2A1.1 were involved in four main processes: cell cycle,  
325 DNA repair, cytoskeleton organization and cell adhesion (S10A, S10B Fig and S4  
326 Table). The two first processes were expected based on earlier studies [21,29,30,39].  
327 However, the relationship between mH2A1.1 and expression of genes involved in  
328 cytoskeleton organization or cell adhesion was undocumented. Using a standard  
329 wide-field microscope, we observed that cells became more elongated after  
330 transfecting two different siRNA against mH2A1.1 (Fig 6A and 6B). We used a siRNA  
331 against mH2A1.2 (S3A-S3C Fig) to test whether this effect was specific of mH2A1.1.  
332 Interestingly, we observed that mH2A1.2 KD cells became rounder compared to  
333 control cells (Fig 6A-6B). Importantly, we noticed that numerous mH2A1.1 KD de-  
334 regulated genes modulate cell migration (examples of anti-migratory genes:  
335 ARRDC3 [40], SOCS4 [41], HACE1 [42] and FBXL4 [43] - and of pro-migratory  
336 genes: EIF6 [44], MT1E [45], JUND [46] and DAPK3 [47]). Thus, we investigated the  
337 effect of mH2A1.1 and mH2A1.2 depletion on the migratory capacity of MDA-MB231  
338 cells using a Boyden Chamber assay (see Materials and Methods). Upon depletion  
339 of mH2A1.1, the migratory capacity of MDA-MB231 cells was significantly increased  
340 compared to control cells. In contrast, depleting the mH2A1.2 isoform led to a  
341 decrease in cell migration (Fig 6C and 6D). Strikingly, mH2A1.1-activated genes  
342 involved in cytoskeleton organization and cell adhesion were also amongst genes  
343 with a high Pol II pausing index (Fig 6E; see Materials and Methods). Taken together,

344 these results suggest that mH2A1.1 inhibits cell migration by in part enhancing the  
345 expression of paused genes involved in cytoskeleton organization and cell adhesion.

346

## 347 **Discussion**

348

349 In this study, we present the first map of the histone variant mH2A1.1 genomic  
350 distribution over the entire human genome in breast cancer cells. Integration of this  
351 map with chromatin features confirms that mH2A1.1, together with its splice variant  
352 mH2A1.2, localizes to “facultative-like” heterochromatin domains and enhancers.  
353 Importantly, for the first time in cancer cells, we identify a direct link between  
354 mH2A1.1 recruitment of transcribed genes and their transcriptional regulation. The  
355 impact of this recruitment on the transcriptional rate is functionally dichotomous, with  
356 positive or negative effects. This bivalence correlates with a differential distribution of  
357 mH2A1.1 around the TSS as well as to the level of dependency of the transcribed  
358 gene to the Pol II pausing.

359

360 The results of our mH2A1 ChIP-seq analysis are overall consistent with  
361 previously published reports identifying this histone variant as a widespread  
362 chromatin feature on autosomes, covering large domains, with a preferential  
363 recruitment to H3K27me3-decorated “facultative-like” heterochromatin (Fig 1C)  
364 [8,9,14,48]. Our mH2A1.1 ChIP-seq analysis allows us to show that even if mH2A1.1  
365 distribution is mainly reminiscent of that of mH2A1.2, each variant has also specific  
366 heterochromatin localizations. Genome mapping of mH2A1.2 is not yet possible due  
367 to the poor specificity or lack of precipitation efficacy of commercial antibodies.

368 We further demonstrate that mH2A1.1-bound chromatin co-localizes  
369 significantly with the H3K9me3 histone mark (Fig 1C). A fraction of these sites are  
370 devoid of H3K27me3 and could correspond to the recently identified macroH2A  
371 localization at constitutive heterochromatin<sup>8</sup>. However, the vast majority of mH2A1.1-  
372 bound H3K9me3-decorated chromatin contained also tri-methylated H3K27 (Fig 1C).  
373 This difference may be a feature of the MDA-MB231 cell line, a high migratory  
374 capacity cancer cell line in which there is an abnormal expansion of frequently  
375 overlapping H3K9me3 and H3K27me3 marks along the genome [49,50].

376 Moreover, we noted that even though mH2A1.1 associates with  
377 heterochromatin domains, its partial loss alone is not sufficient to reactivate silenced  
378 genes present in these domains (S8 Fig). Similarly, even if mH2A1 binding was  
379 shown to overlap with H3K27me3 modified chromatin in primary human cells, no  
380 enrichment of H3K27me3 at mH2A1-regulated genes was observed [14].  
381 Furthermore, mH2A1.2-occupied and repressed target genes are not reactivated  
382 upon mH2A1.2 knock-down [13]. These observations suggest that enrichment of  
383 both mH2A1 isoforms in heterochromatin domains may serve as a lock to conserve  
384 heterochromatin stability and architecture [9].

385

386 In parallel, we show that the depletion of mH2A1.1 alone is sufficient to alter  
387 the expression of many genes present in chromatin domains devoid of H3K27me3  
388 (Figs 4A and S8C). Previous work identified a role for mH2A1.1 in the transcriptional  
389 rate of genes encompassed in H2B acetylated regions but this mechanism was  
390 described as specific of primary cells and absent from cancer cells [14]. Here, we  
391 demonstrate that the effect of mH2A1.1 depletion correlates with the distribution of  
392 mH2A1.1 along transcribed genes. Indeed, mH2A1.1 binding is restricted to the

393 TSSs of mH2A1.1-activated genes while mH2A1.1 binds both upstream and on the  
394 gene body of mH2A1.1-repressed genes (Fig 4B). Our findings reinforce the notion  
395 that mH2A1.1 has a dual role in gene regulation and this seems to depend on its  
396 distribution on mH2A1.1-regulated genes [14]. Molecular mechanisms determining  
397 mH2A1.1 differential localization and the consequent effects on gene regulation  
398 should now to be determined. Perhaps, mH2A1.1 post translational modifications  
399 favor binding to the TSS of active genes. Indeed, mH2A1-S137 phosphorylation  
400 excluded mH2A1 from the inactive X chromosome [51]. Specific protein partners  
401 could also be involved in the recruitment of mH2A1.1 to the TSSs of transcribed  
402 genes, for instance PARP1. Indeed, association of mH2A1.1 and PARP1 was shown  
403 to be involved in gene transcription, DNA repair and global cellular metabolism  
404 [14,18,29].

405 The vast majority of mH2A1.1 narrow peaks at TSSs was only recognized by  
406 our home-made antibody Ab  $\alpha$ mH2A1.1 (Fig 3). We think that this is certainly due to  
407 the high affinity of Ab  $\alpha$ mH2A1.1 towards mH2A1.1 compared to Ab  $\alpha$ mH2A1 (S1F-  
408 S1H Fig). The quantity of mH2A1.1-restricted to the TSSs is significantly smaller than  
409 in the large domains, such as heterochromatin and SEs (Figs 1D,2C and 3C).  
410 Therefore, Ab  $\alpha$ mH2A1 is certainly less efficient in immunoprecipitating mH2A1.1 in  
411 this context. Having a high affinity antibody led us to investigate new localizations  
412 and functions of the mH2A1.1 isoform. Now, it will be interesting to have a high  
413 affinity antibody against mH2A1.2. Indeed, through native-ChIP-seq experiments  
414 using a mH2A1.2 custom-made specific antibody, Dimitris Thanos and his  
415 collaborators recently showed that mH2A1.2 binds to the TSSs of transcribed genes  
416 in human embryonic stem cells [23]. Thus, adapted sequencing techniques, isoform-  
417 specific antibodies and appropriate extractions of mH2A1 chromatin sub-complexes

418 will enable studying mH2A1 splicing isoforms in different chromatin- and cell-  
419 dependend contexts.

420 Interestingly, we remarked that mH2A1.1 TSS-binding is distributed in a  
421 uniform manner around the TSS placing the maximum binding to the nucleosome  
422 free region (NRF) (Fig 3E). Its localization around the TSSs was also observed for  
423 mH2A1.2 using Native ChIP-seq [23], eliminating the hypothesis of a technical bias.  
424 The long- and unstructured- linker domain places the macro domain of mH2A1  
425 outside nucleosomes [6]. Because antibodies against mH2A1 frequently recognize  
426 the linker or the macro domain (as Ab  $\alpha$ mH2A1.1 and Ab  $\alpha$ mH2A1, respectively), we  
427 hypothesize that mH2A1.1 is incorporated at the two adjacent nucleosomes of the  
428 TSSs but their macro domain could be joined at the NFR, which could explain the  
429 higher signal at the NFR compared to the two adjacent nucleosomes. Future analysis  
430 will be necessary to confirm this hypothesis.

431

432 At the cellular level, we observed that the silencing of mH2A1.1 promotes cell  
433 migration, whereas mH2A1.2 silencing increases migration in the MDA-MB231  
434 breast cancer cell line. mH2A1 has been shown to be involved in cell migration in  
435 mouse [52,53] and human [52–55] models. The opposite roles of both splice variants  
436 on the migratory capacities that we see are in agreement with observations in  
437 previous studies using gastric cancer cells [55] and MDA-MB231 cells [52]. At the  
438 molecular level, the selective incorporation of mH2A1.2 along the SOD3 gene  
439 (playing a part in cell migration) has been shown to be directly linked to gene  
440 repression in mouse metastatic cells [52]. Here, we show that the migratory  
441 capacities of human metastatic breast cancer cells are directly regulated by selective  
442 recruitment of mH2A1.1. Among mH2A1.1-activated genes were genes responsible

443 for inhibiting cell migration. Thus, it is tempting to speculate that the negative effect of  
444 mH2A1.1 on cell migration is due to mH2A1.1-dependent activation of genes  
445 inhibiting migration. Interestingly, even if mH2A1.2 is very similar to mH2A1.1 in  
446 terms of amino-acid sequence, it has an opposite function to mH2A1.1 in the  
447 regulation of cell migration. Possibly the NAD<sup>+</sup> metabolite binding pocket of mH2A1.1  
448 plays a role in directing function. Here, we decipher in part the molecular mechanism  
449 by which mH2A1.1 could inhibit cell migration. Taken together, our data reveals  
450 antagonistic cellular functions of both mH2A1 isoforms and highlight the need to  
451 distinguish these isoforms when studying the role of mH2A1.

452

453 We demonstrate that mH2A1.1 favors expression of paused genes (70% of  
454 mH2A1.1-activated genes) (Fig 5E). It will be now interesting to dissect the molecular  
455 mechanisms that allow mH2A1.1 to promote transcription of paused genes. Perhaps,  
456 mH2A1.1 binding to the TSS could stimulate the recruitment of P-TEFb (Positive  
457 Transcription Elongation Factor) and consequently allow Pol II release [38]. PARP1,  
458 well known partner of mH2A1.1, is also involved in Pol II pausing release by  
459 mediating ADP-ribosylation of NELF (Negative elongation factor) [56] and could be  
460 recruited by mH2A1.1. This hypothesis could also explain why we observed  
461 mH2A1.1 at the TSS of highly transcribed genes (Fig 3B and 3D). The presence of  
462 mH2A1.1 at SEs could also induce Pol II release (Fig 2C and 2D). SEs are involved  
463 in cellular identity through the regulation of key genes involved in cellular identity  
464 [36,57]. Furthermore, SEs are known to play an important part in many diseases,  
465 including several cancers<sup>51-53</sup> in which they drive expression of oncogenes [37,58].  
466 To note, several clinical trials already utilize SE blockers (bromodomain and extra-  
467 terminal motif (BET) inhibitor and CDK7i) [59]. Among them, BRD4, one of the BET

468 protein family members, was targeted. BRD4 binds acetylated histones at TSSs and  
469 SEs, brings them together, and mediates transcriptional activation and elongation by  
470 RNA Pol II [37,58]. Interestingly, we observed that 74% of SEs are bound by  
471 mH2A1.1 and BRD4 in MDA-MB231 cells (*data not shown*). Could the presence of  
472 mH2A1.1 at SEs and TSSs be involved in the recruitment of BRD4 to enable  
473 elongation of RNA Pol II on paused mH2A1.1-activated genes ?

474

475 Overall, we demonstrate for the first time that mH2A1.1 activates transcription  
476 of paused genes by its selective recruitment to their TSSs. It remains to demonstrate  
477 whether mH2A1.1 is directly involved in the recruitment of factors acting on Pol II  
478 pausing events and/or on the establishment of 3D-chromatin structures (e.g  
479 chromatin looping mechanisms), facilitating Pol II pausing release.

480

## 481 **Materials and Methods**

482

483 **Cell culture.** MDA-MB231, HEK-293T and MCF7 cell lines were purchased from  
484 ATCC, and were maintained and amplified in Dulbecco's Modified Eagle's (DMEM)  
485 for HEK-93T and MDA-MB231 cells, and in DMEM-F12 for MCF7 cells,  
486 supplemented with gentamycin (50 µg/ml) (Gibco), fetal bovine serum (10%, Gibco)  
487 and sodium pyruvate (100 mM, Sigma). Cells were maintained in a humidified  
488 incubator at 37°C with 5% CO<sub>2</sub>. Cells lines were regularly tested for mycoplasma  
489 infection (MycoAlert, Lonza). In Montpellier, MDA-MB231 cells were cultured in  
490 DMEM supplemented with 10% fetal calf serum and penicillin/streptomycin (100  
491 µg/ml each) and regularly tested for mycoplasma infection.

492 **Transfection of siRNAs and plasmids.** At 30-50% cell confluence, transfection of  
493 siRNA (11nM) was performed using INTERFERin (Polyplus-Ozyme) according to the  
494 manufacturer's protocol. Cells in control condition were transfected with INTERFERin  
495 without any siRNA Transfection of plasmid (1µg) was done with FuGene HD  
496 (Promega) according to the manufacturer's protocol. siRNA and plasmid sequences  
497 are available in S5 Table. Two and three days post plasmid and siRNA transfection  
498 respectively, cells were recovered for experiments.

499 **Western blotting.** Cells were lysed and subjected to western blot analysis as  
500 previously described [60]. Briefly, proteins extracts were separated in 10%  
501 polyacrylamide (1:125 bisacrylamide:acrylamide) SDS gels, transferred onto  
502 nitrocellulose membrane (Bio-Rad) and blocked with PBS-Tween 0.4% - Milk 5% for  
503 1h at RT with rotation. Membranes were then incubated with primary antibodies  
504 overnight (O/N) at 4°C in PBS-Tween 0.4% - Milk 5% with rotation (or 1h30 at RT).  
505 Primary antibodies are described in the S1 Table Membranes were next incubated  
506 with secondary antibody in PBS-Tween 0.4% - Milk 5% 1h at RT with rotation and the  
507 signal was detected using chemiluminescence. Secondary antibodies are described  
508 in the S1 Table. Signal quantifications were carried out with Image Lab software (Bio-  
509 Rad).

510 **RNA extraction, reverse transcription and quantitative real-PCR (qRT-PCR).**  
511 Total RNA was isolated using the RNAeasy midi kit (Qiagen). Purified RNA was  
512 reversed transcribed to cDNA using Maxima H Minus first Strand cDNA synthesis kit  
513 (Promega). The sequences of the primers used are available in S6 Table. RT-PCR  
514 was performed using iTAq Universal SYBR Green (Bio-Rad) according to  
515 manufacturer's instructions. At least two independent experiments were performed

516 for each condition. The relative expression levels of mRNA were normalized to  
517 RPLP0 mRNA expression and evaluated according to the  $2^{-\Delta\Delta Ct}$  method [61].

518 **Fluorescence microscopy.** Two or three days post-transfection, cells were fixed  
519 with 4 % paraformaldehyde for 15 min for MDA-MB231 cells and 10 min for HEK-  
520 293T at RT. Cells permeabilization was carried out using 0.1 % Triton X-100 in PBS  
521 for 10 min at RT. Cells were then blocked with 5 % BSA-0.15% Tween in PBS for 1h  
522 at RT. Next, cells were incubated with primary antibody O/N at 4°C. Cells were then  
523 incubated with Alexa conjugated secondary antibody for 1h at RT. Actin was labelled  
524 using cytoPainter Phalloidin iFluor diluted 1:1000 with secondary antibody according  
525 to the manufacturer's protocol (Abcam; see S1 Table). Antibodies references and  
526 dilutions are provided in S1 Table. The coverslips were finally incubated with Hoechst  
527 (Invitrogen, 33342) for 30 min and then mounting with mounting media (Vectashield).  
528 Images were acquired with Zeiss LSM 710 big confocal microscope using an x63 PL  
529 APO oil DIC On 1.4 objective for all experiments. Images were taken in Z-stacks with  
530 a voxel size of 300 nm. A Z-stack or Standard deviation intensity projections of Z-  
531 stacks are shown.

532 **Chromatin immunoprecipitation and library preparation.** Cells were cross-linked  
533 in DMEM containing 1.2 % of paraformaldehyde at RT for 10 min with rotation.  
534 Cross-link was stopped by the addition of glycine to a final concentration of 0.125M  
535 for 5 min. Cell were harvested and lysed in cell lysis buffer (10 mM Tris-HCl pH 7.4,  
536 15 mM NaCl, 60 mM KCL, 1 mM EDTA, 0.1 mM EGTA, 0.2% NP-40, 5% sucrose).  
537 After 10 min in ice, cell lysis was amplified with a 2mL dounce (Kimble Chase) to  
538 enhance the nuclei separation from cytoplasm. Cell lysis buffer containing lysed cells  
539 was deposit up to a pillow buffer (10 mM Tris-HCl pH 7.4, 15 mM NaCl, 60 mM KCL,  
540 1 mM EDTA, 0.1 mM EGTA, 0.2% NP-40, 10% sucrose). Nuclei were then pelleted

541 by centrifugation and wash with washing buffer (10 mM Tris-HCl pH 7.4, 15 mM  
542 NaCl, 60 mM KCL). Nuclei were then resuspended in sonication buffer (50 mM Tris-  
543 HCl pH 7.5, 150 mM KCl, 5 mM EDTA, 1% NP-40, 0.1% SDS, 0.5 % Sodium  
544 deoxycholate, Protease Inhibitor (Roche)). Chromatin was sheared using a Bioruptor  
545 (Diagenode) (30 cycles, 30 sec ON/ 30 sec OFF) in order to obtain chromatin  
546 fragments with an average size of 300-500 bp. Quality and size of chromatin  
547 fragments was monitored by ethidium-bromide stained agarose gel electrophoresis  
548 after DNA purification. Then, 100 µg of DNA was incubated with antibody O/N at 4°C  
549 on a rotation wheel. Antibodies are described in the S1 Table. 3 mg of protein A  
550 magnetic dynabeads (Sigma) were added for 3h at 4°C on a rotation wheel.  
551 Immunoprecipitates were then exposed to serial washes for 5 min each on a rotation  
552 wheel at 4°C in the following buffers (two times/buffer) : WB<sub>I</sub>: 2 mM EDTA, 20 mM  
553 Tris pH 8.1, 1 % Triton 100X, 150 mM NaCl, WB<sub>II</sub>: 2 mM EDTA, 20 mM Tris pH 8.1, 1  
554 % Triton X100, 500 mM NaCl, WB<sub>III</sub>: 1 mM EDTA, 10 mM Tris pH 8.1, 250 mM LiCl,  
555 1 % Sodium deoxycholate, 1 % NP-40 and WB<sub>IV</sub>: 1 M EDTA, 10 mM Tris pH 8.1.  
556 Chromatin was eluted from the magnetic beads with DNA isolation buffer (2% SDS,  
557 0.1 M NaHCO<sub>3</sub>) for 1h at 65°C under agitation. Extracts were reverse-crosslinked  
558 with SDS O/N at 65°C. RNAs were degraded with RNase A and proteins were finally  
559 degraded with proteinase K. Same procedure was performed for input (10 µg of  
560 DNA). DNA was finally extracted with a phenol-chloroform extraction. Quantity and  
561 quality of DNA was tested with a nanodrop (NanoDrop2000, Thermo). Samples were  
562 sequenced with the GeT core facility, Toulouse, France (<http://get.genotoul.fr>).  
563 Sequencing was done HiSeq3000-HWI-J00115 according to the manufacturer's  
564 protocol. Same procedure was done for ChIPqPCR, expected that 20 µg of DNA was  
565 used with 1µg of antibody). The sequences of the primers used are available in

566 Supplementary Table 7. For western blot analysis, extracts (Input (10% IP), No  
567 immunoprecipitated (NoIP) fraction and IP fraction were processed as ChIP extract  
568 but not incubated with the proteinase K and RNAase A. Extracts were then subjected  
569 to western blot analysis as previously described in the western blot paragraph. To  
570 compare different extracts, we loaded 2 % of Input, 0.5 % of Input, 0.5 % of NoIP  
571 fraction and 20% of IP fraction. Percentages are relative to the DNA quantity used for  
572 ChIP (100 µg).

573 ChIP-seq of H3K27ac, H3K4me1, H3K4me3, H3K36me3 and Pol II were done  
574 essentially as previously described [62]. Briefly, after cell fixation with 1 % of  
575 paraformaldehyde at RT for 5 min, cells were incubated in cell lysis buffer (PIPES 5  
576 mM, KCL 85 mM, NP40 0.5%, Na Butyrate 10 mM, protease inhibitors) for 10 min on  
577 ice. After mild centrifugation, nuclei were lysed in Nuclei Lysis Buffer (Tris-HCL 50  
578 mM pH 7.5, SDS 0.125%, EDTA 10 mM, Na Butyrate 10 mM, protease inhibitors) at  
579 4°C for 2h and, then, sonicated for 10 cycles at 4°C using BioruptorPico device from  
580 Diagenode. For immunoprecipitation of H3K4me1, H3K4me3 and H3K27ac, 150 µl of  
581 chromatin (equivalent to  $4 \cdot 10^6$  cells) and 4.5 µg of the corresponding antibodies were  
582 used. For Pol II, 850 µl of chromatin (equivalent to  $22 \cdot 10^6$  cells) and 20 µg of the  
583 corresponding antibody were used. Two independent replicates for each ChIP were  
584 sequenced by the MGX genomic platform (Montpellier) using the Hi-seq2500 Illumina  
585 sequencer.

586 **Strand-specific total RNA library preparation.** Total RNA was isolated using the  
587 RNAeasy midi kit (Qiagen). RNA-seq quality and quantity control were performed  
588 using a Nanodrop (NanoDrop2000, Thermo) and BioAnalyser. Library preparation  
589 and sequencing was done by GeT core facility, Toulouse, France  
590 (<http://get.genotoul.fr>) with the kit TruSeq Stranded total RNA according to

591 manufacturer's institutions. Sequencing was done HiSeq3000-HWI-J00115 according  
592 to the manufacturer's protocol.

593 **ChIP-seq data processing.** The quality of the reads was estimated with FastQC  
594 (Illumina, 1.0.0). Published ChIP-seq data of H3K9me3 (GSM2258862), H3K27me3  
595 (GSM2258850) and corresponding input (GSM2258864) in MDA-MB231 cells were  
596 downloaded from GEODATASETS (<https://www.ncbi.nlm.nih.gov/geo/>, GEO  
597 accession number : GSE85158) [33], and reanalyzed as subsequently described.  
598 Published ChIP-seq data of BRD4 in MDA-MB231 cells were downloaded  
599 (GSM2862187) and corresponding input (GSM2862178) from GEODATASETS  
600 (<https://www.ncbi.nlm.nih.gov/geo/>, GEO accession number : GSE107176) [63], and  
601 reanalyzed as subsequently described. Sequenced reads were aligned to the human  
602 genome Assembly GRCh38 using STAR (2.5.1) algorithm with defaults  
603 parameters[64]. Details are supplied in Supplementary Table 2. Low quality reads  
604 were then filtered out using Samtools (Samtools, options `-q 10 -view`) [65].  
605 Conversion of BAM files to bigWig files was performed with Bamcompare tool  
606 (DeepTools utilities v3.1.3) [66]. Corresponding ChIP-seq data generated from  
607 genomic DNA (Input) were used as control for every bigWig files normalization  
608 (options: `--normalizeUsing RPKM --operation subtract --binSize 50 bp --`  
609 `smoothLength 150 bp`). Peaks were determined with the enrichR function of NormR  
610 package [67] (v3.8, Options: `fdr = 5e-2, binsize = 500 bp` for H3K27ac, H3K4me1,  
611 H3K4me3, BRD4 and `binsize =3000 bp` for H3K36me3, PolII, H3K9me3, H3K27me3,  
612 Ab  $\alpha$ H2A1.1 and Ab  $\alpha$ H2A1). Peaks of Ab  $\alpha$ H2A1.1 (and Ab  $\alpha$ H2A1) spaced  
613 less than 3000 bp on the linear genome were merged. All downstream analyses were  
614 mainly performed with R studio. ChIP-seq signal and peaks positions visualization  
615 were obtained with IGV [68,69]. Boxplots were done with ggplot2 [70]. Distributions of

616 mH2A1 isoforms and H3K27me3/H3K9me3 common peaks identified at specific  
617 genomic features were calculated using ChIPseeker package with default  
618 parameters (Figs 1B and S5B) [71]. Statistical analyses are presented in Statistics  
619 and Reproducibility paragraph.

620 **Identification of “putative” enhancers and super-enhancers.** All putative  
621 enhancers correspond to the union of H3K4me1 and H3K27ac outside TSS (+/- 2 kb)  
622 to avoid TSS bias (Fig 2B) [72]. TSS annotation is based on  
623 TxDb.Hsapiens.UCSC.hg38.knownGene release. Super-enhancers were determined  
624 with ROSE utility tools based on H3K27ac signal (options : stitching\_distance = 12.5  
625 kb and TSS\_exclusion\_zone\_size : 2500 bp) (Fig 2C and 2D) [36,37].

626 **Pol II pausing index calculation.** Pausing index (PI) was defined as previously[73],  
627 which is the ratio of Pol II (total) density in the promoter-proximal region ([-30;300] bp  
628 centered on TSS) to the total Pol II density in the transcribed regions (TSS + 300 bp  
629 to TES). Pausing index was only calculated for actively expressed genes (n=10,198,  
630 see RNA-seq analysis). Paused genes were defined as genes that have a PI upper  
631 to 2 (n=6,821).

632 **Venn diagrams.** Intersection of peaks were determined with the function  
633 findOverlaps() from GenomicRanges package. To note that for two ChIP-seq peaks  
634 intersections, only number of overlaps is contabilised and not the number of each  
635 peaks contained per overlap. This particularity explained why number of peaks  
636 changes between venn diagrams for a same ChIP-seq (i.e Fig 1A Ab  $\alpha$ mH2A1.1  
637 (n=29,112) and Fig 1C  $\alpha$ mH2A1.1 (n=19,867)). The area-proportional Venn diagrams  
638 were drawn based on images generated by Vennable package. For Venn diagrams  
639 in Fig 3, 5 and S6, intersections were performed at TSS (1-bp or +/- 1kb centered on

640 TSS). Enrichment tests associated to Venn diagrams are explained in Statistics and  
641 Reproducibility paragraph.

642 **Correlation heatmaps.** Correlation heatmaps were done with multiBigwigSummary  
643 (options: -bins for whole genome (S2A Fig) or -BED-file for Heterochromatin,  
644 enhancer, TSS +/-1kp; TSS 1-bp, Figs S2B, S6A and S7B ) and plotCorrelation  
645 (option: -spearman correlation heatmap) from DeepTools utilities (3.1.3) [66].

646 **Metagenes profils.** Metagene analysis profiles were performed with R Seqplot  
647 package using bigWig files (function getPlotSetArray and plotAverage) [74].  
648 Heatmaps profiles of Pol II, Ab  $\alpha$ H2A1.1 and Ab  $\alpha$ H2A1 around TSS +/- 10 kb  
649 were ranked by mH2A1.1 KD de-regulated genes (mH2A1.1-activated and repressed  
650 genes, not ranked by the deregulation level) and done with Seqplot package  
651 (function getPlotSetArray and plotHeatmap) (Fig 4B). Heatmaps profiles of Pol II, Ab  
652  $\alpha$ H2A1.1 and Ab  $\alpha$ H2A1 around TSS +/- 10 kb were ranked by pausing index and  
653 carried out with Seqplot package (function getPlotSetArray and plotHeatmap)(Fig  
654 5A).

655 **RNA-seq analysis.** The quality of the reads was estimated with FastQC (Illumina,  
656 1.0.0). The reads were mapped to the human reference genome GRCh38 using the  
657 default parameters of STAR (2.5.1) [64]. Details are supplied in S1 Table . Low  
658 quality reads and duplicates were then filtered out using SAMtools (Samtools,  
659 options -q 10 -view ; -rmdup)[65]. Unstranded normalized Bedgraph files in Read Per  
660 Millions (RPM) were obtained with STAR using Output Wiggle parameters (options : -  
661 -outWigTypebedgraph; --outWigStrandUnstranded; --outWigNorm RPM) [64]. Gene  
662 counts were performed with htseq-count utilities with default parameters (0.8.0) [74].  
663 FPKM for all genes were calculated with the formula :  $FPKM = (RC_g \times 10^6) / (RC_p \times L)$   
664 where  $RC_g$  corresponds to the number of reads mapped to the gene,  $RC_p$  to the

665 number of reads mapped to all protein-coding genes and L, the Length of the gene in  
666 base pairs. Differential expression analysis was performed with DESeq2 package  
667 [75] with cutoff  $|FC| > 1.5$  and  $padj < 0.1$ . Corresponding volcano plot was done with  
668 EnhancedVolcano package [76] (Fig 4A). The mH2A1.1 KD de-regulated genes are  
669 listed in S3 Table.

670 **GO analysis.** GO analysis was performed with LIMMA package (--function goana)  
671 (3.8)[77] and corresponding GO terms are supplied in the S4 Table. Selection of  
672 genes related to their functions was done with biomaRt package (function getBM())  
673 [78,79]. We took genes related to: cytoskeleton (GO:0005856), cell adhesion  
674 (GO:0007155), Cilium (GO:0005929) and cell junction (GO:0030054) (n=6,821).

675 **Transwell migration assay.** Transwell migration assays were performed using  
676 Transwell plates with 0.8  $\mu\text{m}$  pore polycarbonate membranes (CorningTranswell,  
677 Sigma). Three days post siRNA transfection, MDA-MB231 cells ( $10^5$ ) were seeded in  
678 the upper chamber without FBS and allowed to invade to the reverse side of the  
679 chamber under chemoattractant condition with 10% FBS medium in the lower  
680 chamber. Following incubation for 16h at 37°C, the cells were fixed with 3.7%  
681 formaldehyde for 2 min at RT. Cells permeabilization was carried out with methanol  
682 incubation for 20 min at RT. Cells were then stained with Giesma for 15 min at RT.  
683 Same final total cell number between conditions was always checked by wide field  
684 microscope to avoid proliferation bias during number of migratory cell comparison.  
685 Not migrated cells were finally removed from the upper chamber by using a cotton  
686 swab. Migrated cells adhering to the underside of the chamber were photographed  
687 using a light microscope at x200 magnification (Invitrogen EVOS Digital Color  
688 Fluorescence Microscope). Cell counting was done with ImageJ in ten different fields

689 per condition[80]. Three independent experiments were performed for each  
690 condition.

691 **Statistics and reproducibility.** All western blot, RTqPCR and Boyden Chamber  
692 assay experiments were repeated at least twice as independent biological replicates  
693 and results are presented as mean +/- sd. All statistical analyses were done with R.  
694 For Western blot, RTqPCR and Boyden Chamber, Wilcoxon tests were used to  
695 compare mean values between conditions. p-values were considered as significant  
696 when \*  $\leq 0.05$  and highly significant when \*\*  $\leq 0.01$ ; \*\*\*  $\leq 0.001$ ; \*\*\*\*  $\leq 0.0001$ . All  
697 enrichment tests were performed on a base set made up of genomic bins. Each  
698 genomic bin is defined by merging ranges of ChIP-seq data (reduce function  
699 GenomicRanges R package) ChIP-seq list : Ab  $\alpha$ H2A1.1, Ab  $\alpha$ H2A1, Pol II,  
700 H3K4me3, H3K4me1, H3K36me3, H3K27ac, H3K27me3, H3K9me3, “putative”  
701 enhancers and “putative” Super-enhancers, on whole genome or TSS +/- 1kb and  
702 TSS 1-bp.

703

704 **Data availability.** ChIP-seq and RNA-seq data have been deposited to GEO under  
705 accession number GSE140022. Additional data are available upon reasonable  
706 request.

707

## 708 **Acknowledgements**

709 We thank M. Buschbeck from JCLR Institute at Barcelona for kindly providing Flag-  
710 mH2A1.1 and Flag-mH2A1.2 expression plasmids. ChIP-seq data against mH2A1.1  
711 and mH2A1 isoforms as well as RNA-seq data were performed in collaboration with  
712 the GeT core facility, Toulouse, France (<http://get.genotoul.fr>), and were supported  
713 by France Génomique National infrastructure, funded as part of “Investissement

714 d’avenir” program managed by Agence Nationale pour la Recherche (contract ANR-  
715 10-INBS-09) and by the Fondation Recherche Medical (DEQ43940 to O.C team  
716 including A.H). We thank Marc Piechaszky for critical reading of the manuscript. We  
717 acknowledge support from the light imaging Toulouse CBI platform. The work was  
718 generously funded by the Institut National du Cancer (INCA PL-BIO-16-269) to KB.

719

## 720 **Author contributions**

721 L.R, A-C.L and K.B conceived this study. F.M validated custom Ab  $\alpha$ mH2A1.1  
722 antibody specificity against mH2A1.1. L.R performed ChIP-seq against mH2A1  
723 isoforms and RNA-seq. I.E-J. and F.B performed ChIP-seq against active histone  
724 marks. L.R, A.H and F.R realized bioinformatic analysis of all ChIP-seq and RNA-seq  
725 data. Statistical analyses were done by A.H and L.R. L.R performed all other  
726 experimental data. L.R, A-C.L and K.B designed experiments and interpreted results.  
727 L.R, A-C.L and K.B wrote the manuscript with input from all other authors.

728

## 729 **Competing interests**

730

731 The authors declare no competing interests.

732

## 733 **References**

- 734 1. Venkatesh S, Workman JL. Histone exchange, chromatin structure and the  
735 regulation of transcription. *Nat Rev Mol Cell Biol* [Internet]. 2015 Mar 4 [cited  
736 2019 Nov 6];16(3):178–89. Available from:  
737 <http://www.ncbi.nlm.nih.gov/pubmed/25650798>
- 738 2. Luger K, Dechassa ML, Tremethick DJ. New insights into nucleosome and

- 739 chromatin structure: an ordered state or a disordered affair? *Nat Rev Mol Cell*  
740 *Biol* [Internet]. 2012 Jul 22 [cited 2019 Jul 23];13(7):436–47. Available from:  
741 <http://www.ncbi.nlm.nih.gov/pubmed/22722606>
- 742 3. Buschbeck M, Hake SB. Variants of core histones and their roles in cell fate  
743 decisions, development and cancer. *Nat Rev Mol Cell Biol* [Internet]. 2017 Feb  
744 1 [cited 2017 May 10];18(5):299–314. Available from:  
745 <http://www.ncbi.nlm.nih.gov/pubmed/28144029>
- 746 4. Pehrson JR, Fuji RN. Evolutionary conservation of histone macroH2A subtypes  
747 and domains. *Nucleic Acids Res* [Internet]. 1998 Jun 15 [cited 2019 Jul  
748 23];26(12):2837–42. Available from: [https://academic.oup.com/nar/article-](https://academic.oup.com/nar/article-lookup/doi/10.1093/nar/26.12.2837)  
749 [lookup/doi/10.1093/nar/26.12.2837](https://academic.oup.com/nar/article-lookup/doi/10.1093/nar/26.12.2837)
- 750 5. Rivera-Casas C, Gonzalez-Romero R, Cheema MS, Ausió J, Eirín-López JM.  
751 The characterization of macroH2A beyond vertebrates supports an ancestral  
752 origin and conserved role for histone variants in chromatin. *Epigenetics*  
753 [Internet]. 2016 Jun 2 [cited 2019 Jul 23];11(6):415–25. Available from:  
754 <http://www.tandfonline.com/doi/full/10.1080/15592294.2016.1172161>
- 755 6. Gamble MJ, Kraus WL. Multiple facets of the unique histone variant  
756 macroH2A: From genomics to cell biology. *Cell Cycle*. 2010;9(13):2568–74.
- 757 7. Costanzi C, Pehrson JR. Histone macroH2A1 is concentrated in the inactive X  
758 chromosome of female mammals. *Nature*. 1998;628(1997):1997–9.
- 759 8. Gamble MJ, Frizzell KM, Yang C, Krishnakumar R, Kraus WL. The histone  
760 variant macroH2A1 marks repressed autosomal chromatin, but protects a  
761 subset of its target genes from silencing. *Genes Dev* [Internet]. 2010 Jan 1  
762 [cited 2019 Jul 23];24(1):21–32. Available from:  
763 <http://genesdev.cshlp.org/cgi/doi/10.1101/gad.1876110>

- 764 9. Douet J, Corujo D, Malinverni R, Renauld J, Sansoni V, Posavec Marjanović  
765 M, et al. MacroH2A histone variants maintain nuclear organization and  
766 heterochromatin architecture. *J Cell Sci.* 2017;130(9):1570–82.
- 767 10. Sun Z, Filipescu D, Andrade J, Gaspar-Maia A, Ueberheide B, Bernstein E.  
768 Transcription-associated histone pruning demarcates macroH2A chromatin  
769 domains. *Nat Struct Mol Biol [Internet].* 2018 Oct 5 [cited 2019 Jul  
770 23];25(10):958–70. Available from: [http://www.nature.com/articles/s41594-018-](http://www.nature.com/articles/s41594-018-0134-5)  
771 0134-5
- 772 11. Doyen C-M, An W, Angelov D, Bondarenko V, Mietton F, Studitsky VM, et al.  
773 Mechanism of polymerase II transcription repression by the histone variant  
774 macroH2A. *Mol Cell Biol [Internet].* 2006 Feb 1 [cited 2019 Jul 23];26(3):1156–  
775 64. Available from: [http://mcb.asm.org/cgi/doi/10.1128/MCB.26.3.1156-](http://mcb.asm.org/cgi/doi/10.1128/MCB.26.3.1156-1164.2006)  
776 1164.2006
- 777 12. Angelov D, Molla A, Perche P-Y, Hans F, Côté J, Khochbin S, et al. The  
778 histone variant macroH2A interferes with transcription factor binding and  
779 SWI/SNF nucleosome remodeling. *Mol Cell [Internet].* 2003 Apr [cited 2019 Jul  
780 23];11(4):1033–41. Available from:  
781 <http://www.ncbi.nlm.nih.gov/pubmed/12718888>
- 782 13. Dell'Orso S, Wang AH, Shih H-Y, Saso K, Berghella L, Gutierrez-Cruz G, et al.  
783 The Histone Variant MacroH2A1.2 Is Necessary for the Activation of Muscle  
784 Enhancers and Recruitment of the Transcription Factor Pbx1. *Cell Rep*  
785 [Internet]. 2016 Feb 9 [cited 2019 Jul 23];14(5):1156–68. Available from:  
786 <https://linkinghub.elsevier.com/retrieve/pii/S2211124716000036>
- 787 14. Chen H, Ruiz PD, Novikov L, Casill AD, Park JW, Gamble MJ. MacroH2A1.1  
788 and PARP-1 cooperate to regulate transcription by promoting CBP-mediated

- 789 H2B acetylation. *Nat Struct Mol Biol* [Internet]. 2014 Oct 12 [cited 2016 Nov  
790 19];21(11):981–9. Available from:  
791 <http://www.nature.com/doi/10.1038/nsmb.2903>
- 792 15. Podrini C, Koffas A, Chokshi S, Vinciguerra M, Lelliott CJ, White JK, et al.  
793 MacroH2A1 isoforms are associated with epigenetic markers for activation of  
794 lipogenic genes in fat-induced steatosis. *FASEB J* [Internet]. 2015 May [cited  
795 2019 Jul 23];29(5):1676–87. Available from:  
796 <http://www.fasebj.org/doi/10.1096/fj.14-262717>
- 797 16. Wan D, Liu C, Sun Y, Wang W, Huang K, Zheng L. MacroH2A1.1 cooperates  
798 with EZH2 to promote adipogenesis by regulating Wnt signaling. *J Mol Cell Biol*  
799 [Internet]. 2017 Aug 1 [cited 2019 Jul 23];9(4):325–37. Available from:  
800 [http://academic.oup.com/jmcb/article/9/4/325/4067698/MacroH2A11-](http://academic.oup.com/jmcb/article/9/4/325/4067698/MacroH2A11-cooperates-with-EZH2-to-promote)  
801 [cooperates-with-EZH2-to-promote](http://academic.oup.com/jmcb/article/9/4/325/4067698/MacroH2A11-cooperates-with-EZH2-to-promote)
- 802 17. Changolkar LN, Singh G, Cui K, Berletch JB, Zhao K, Disteché CM, et al.  
803 Genome-wide distribution of macroH2A1 histone variants in mouse liver  
804 chromatin. *Mol Cell Biol* [Internet]. 2010 Dec 1 [cited 2019 Jul 23];30(23):5473–  
805 83. Available from: <http://mcb.asm.org/cgi/doi/10.1128/MCB.00518-10>
- 806 18. Posavec Marjanović M, Hurtado-Bagès S, Lassi M, Valero V, Malinverni R,  
807 Delage H, et al. MacroH2A1.1 regulates mitochondrial respiration by limiting  
808 nuclear NAD<sup>+</sup> consumption. *Nat Struct Mol Biol* [Internet]. 2017 Nov 9 [cited  
809 2019 Aug 7];24(11):902–10. Available from:  
810 <http://www.nature.com/articles/nsmb.3481>
- 811 19. Sporn JC, Kustatscher G, Hothorn T, Collado M, Serrano M, Muley T, et al.  
812 Histone macroH2A isoforms predict the risk of lung cancer recurrence.  
813 *Oncogene* [Internet]. 2009 Sep 3 [cited 2019 Jul 23];28(38):3423–8. Available

- 814 from: <http://www.ncbi.nlm.nih.gov/pubmed/19648962>
- 815 20. Cantariño N, Douet J, Buschbeck M. MacroH2A – An epigenetic regulator of  
816 cancer. *Cancer Lett* [Internet]. 2013 Aug [cited 2019 Jul 23];336(2):247–52.  
817 Available from: <https://linkinghub.elsevier.com/retrieve/pii/S0304383513002504>
- 818 21. Sporn JC, Jung B. Differential regulation and predictive potential of MacroH2A1  
819 isoforms in colon cancer. *Am J Pathol* [Internet]. 2012 Jun [cited 2019 Jul  
820 23];180(6):2516–26. Available from:  
821 <http://www.ncbi.nlm.nih.gov/pubmed/22542848>
- 822 22. Mermoud JE, Costanzi C, Pehrson JR, Brockdorff N. Histone MacroH2A1 . 2  
823 Relocates to the Inactive X Chromosome after Initiation and Propagation of X-  
824 Inactivation. *J Cell Biol*. 1999;147(7):1399–408.
- 825 23. Pliatska M, Kapasa M, Kokkalis A, Polyzos A, Thanos D. The Histone Variant  
826 MacroH2A Blocks Cellular Reprogramming by Inhibiting Mesenchymal-to-  
827 Epithelial Transition. *Mol Cell Biol* [Internet]. 2018 Feb 15 [cited 2019 Jul  
828 23];38(10):e00669-17. Available from:  
829 <http://mcb.asm.org/lookup/doi/10.1128/MCB.00669-17>
- 830 24. Lavigne A-C, Castells M, Mermet J, Kocanova S, Dalvai M, Bystricky K.  
831 Increased macroH2A1.1 expression correlates with poor survival of triple-  
832 negative breast cancer patients. Haibe-Kains B, editor. *PLoS One* [Internet].  
833 2014 Jun 9 [cited 2019 Jul 23];9(6):e98930. Available from:  
834 <https://dx.plos.org/10.1371/journal.pone.0098930>
- 835 25. Kustatscher G, Hothorn M, Pugieux C, Scheffzek K, Ladurner AG. Splicing  
836 regulates NAD metabolite binding to histone macroH2A. *Nat Struct Mol Biol*  
837 [Internet]. 2005 Jul 19 [cited 2019 Jul 23];12(7):624–5. Available from:  
838 <http://www.ncbi.nlm.nih.gov/pubmed/15965484>

- 839 26. Ray Chaudhuri A, Nussenzweig A. The multifaceted roles of PARP1 in DNA  
840 repair and chromatin remodelling. *Nat Rev Mol Cell Biol* [Internet]. 2017 Oct 5  
841 [cited 2019 Jul 23];18(10):610–21. Available from:  
842 <http://www.ncbi.nlm.nih.gov/pubmed/28676700>
- 843 27. Ouararhni K, Hadj-Slimane R, Ait-Si-Ali S, Robin P, Mietton F, Harel-Bellan A,  
844 et al. The histone variant mH2A1.1 interferes with transcription by down-  
845 regulating PARP-1 enzymatic activity. *Genes Dev* [Internet]. 2006 Dec 1 [cited  
846 2019 Jul 23];20(23):3324–36. Available from:  
847 <http://www.genesdev.org/cgi/doi/10.1101/gad.396106>
- 848 28. Marjanović MP, Hurtado-bagès S, Lassi M, Valero V, Malinverni R, Delage H,  
849 et al. MacroH2A1 . 1 regulates mitochondrial respiration by limiting nuclear  
850 NAD + consumption. 2018;24(11):902–10.
- 851 29. Xu C, Xu Y, Gursoy-Yuzugullu O, Price BD. The histone variant macroH2A1.1  
852 is recruited to DSBs through a mechanism involving PARP1. *FEBS Lett*  
853 [Internet]. 2012 Nov 2 [cited 2019 Jul 23];586(21):3920–5. Available from:  
854 <http://doi.wiley.com/10.1016/j.febslet.2012.09.030>
- 855 30. Kim J, Oberdoerffer P, Khurana S. The histone variant macroH2A1 is a  
856 splicing-modulated caretaker of genome integrity and tumor growth. *Mol Cell*  
857 *Oncol* [Internet]. 2018 Mar 7 [cited 2019 Jul 23];5(3):e1441629. Available from:  
858 <https://www.tandfonline.com/doi/full/10.1080/23723556.2018.1441629>
- 859 31. Chen H, Ruiz PD, McKimpson WM, Novikov L, Kitsis RN, Gamble MJ.  
860 MacroH2A1 and ATM Play Opposing Roles in Paracrine Senescence and the  
861 Senescence-Associated Secretory Phenotype. *Mol Cell* [Internet]. 2015 Sep  
862 [cited 2019 Dec 11];59(5):719–31. Available from:  
863 <https://linkinghub.elsevier.com/retrieve/pii/S1097276515005699>

- 864 32. Ouararhni K, Hadj-Slimane R, Ait-Si-Ali S, Robin P, Mietton F, Harel-Bellan A,  
865 et al. The histone variant mH2A1.1 interferes with transcription by down-  
866 regulating PARP-1 enzymatic activity. *Genes Dev* [Internet]. 2006 Dec 1 [cited  
867 2019 Dec 11];20(23):3324–36. Available from:  
868 <http://www.genesdev.org/cgi/doi/10.1101/gad.396106>
- 869 33. Franco HL, Nagari A, Malladi VS, Li W, Xi Y, Richardson D, et al. Enhancer  
870 transcription reveals subtype-specific gene expression programs controlling  
871 breast cancer pathogenesis. *Genome Res* [Internet]. 2018 Feb [cited 2019 Jul  
872 23];28(2):159–70. Available from:  
873 <http://genome.cshlp.org/lookup/doi/10.1101/gr.226019.117>
- 874 34. Allshire RC, Madhani HD. Ten principles of heterochromatin formation and  
875 function. *Nat Rev Mol Cell Biol* [Internet]. 2018 Apr 13 [cited 2019 Jul  
876 26];19(4):229–44. Available from: <http://www.nature.com/articles/nrm.2017.119>
- 877 35. Creighton MP, Cheng AW, Welstead GG, Kooistra T, Carey BW, Steine EJ, et  
878 al. Histone H3K27ac separates active from poised enhancers and predicts  
879 developmental state. *Proc Natl Acad Sci* [Internet]. 2010 Dec 14 [cited 2019 Jul  
880 23];107(50):21931–6. Available from:  
881 <http://www.pnas.org/cgi/doi/10.1073/pnas.1016071107>
- 882 36. Whyte WA, Orlando DA, Hnisz D, Abraham BJ, Lin CY, Kagey MH, et al.  
883 Master Transcription Factors and Mediator Establish Super-Enhancers at Key  
884 Cell Identity Genes. *Cell* [Internet]. 2013 Apr [cited 2019 Jul 23];153(2):307–19.  
885 Available from: <https://linkinghub.elsevier.com/retrieve/pii/S0092867413003929>
- 886 37. Lovén J, Hoke HA, Lin CY, Lau A, Orlando DA, Vakoc CR, et al. Selective  
887 inhibition of tumor oncogenes by disruption of super-enhancers. *Cell* [Internet].  
888 2013 Apr 11 [cited 2019 Jul 23];153(2):320–34. Available from:

- 889 <https://linkinghub.elsevier.com/retrieve/pii/S0092867413003930>
- 890 38. Adelman K, Lis JT. Promoter-proximal pausing of RNA polymerase II:  
891 emerging roles in metazoans. *Nat Rev Genet* [Internet]. 2012 Oct 18 [cited  
892 2019 Jul 23];13(10):720–31. Available from:  
893 <http://www.ncbi.nlm.nih.gov/pubmed/22986266>
- 894 39. Novikov L, Park JW, Chen H, Klerman H, Jalloh AS, Gamble MJ. QKI-  
895 mediated alternative splicing of the histone variant MacroH2A1 regulates  
896 cancer cell proliferation. *Mol Cell Biol* [Internet]. 2011 Oct 15 [cited 2019 Jul  
897 23];31(20):4244–55. Available from:  
898 <http://mcb.asm.org/cgi/doi/10.1128/MCB.05244-11>
- 899 40. Draheim KM, Chen H-B, Tao Q, Moore N, Roche M, Lyle S. ARRDC3  
900 suppresses breast cancer progression by negatively regulating integrin beta4.  
901 *Oncogene* [Internet]. 2010 Sep 9 [cited 2019 Jul 23];29(36):5032–47. Available  
902 from: <http://www.nature.com/articles/onc2010250>
- 903 41. Mei Z, Chen S, Chen C, Xiao B, Li F, Wang Y, et al. Interleukin-23 Facilitates  
904 Thyroid Cancer Cell Migration and Invasion by Inhibiting SOCS4 Expression  
905 via MicroRNA-25. Zhang Z, editor. *PLoS One* [Internet]. 2015 Oct 5 [cited 2019  
906 Jul 23];10(10):e0139456. Available from:  
907 <https://dx.plos.org/10.1371/journal.pone.0139456>
- 908 42. Castillo-Lluva S, Tan C-T, Daugaard M, Sorensen PHB, Malliri A. The tumour  
909 suppressor HACE1 controls cell migration by regulating Rac1 degradation.  
910 *Oncogene* [Internet]. 2013 Mar 28 [cited 2019 Jul 23];32(13):1735–42.  
911 Available from: <http://www.nature.com/articles/onc2012189>
- 912 43. Stankiewicz E, Mao X, Mangham DC, Xu L, Yeste-Velasco M, Fisher G, et al.  
913 Identification of FBXL4 as a Metastasis Associated Gene in Prostate Cancer.

- 914 Sci Rep [Internet]. 2017 Dec 11 [cited 2019 Jul 23];7(1):5124. Available from:  
915 <http://www.nature.com/articles/s41598-017-05209-z>
- 916 44. Pinzaglia M, Montaldo C, Polinari D, Simone M, La Teana A, Tripodi M, et al.  
917 EIF6 over-expression increases the motility and invasiveness of cancer cells by  
918 modulating the expression of a critical subset of membrane-bound proteins.  
919 BMC Cancer [Internet]. 2015 Mar 15 [cited 2019 Jul 23];15(1):131. Available  
920 from: <http://bmccancer.biomedcentral.com/articles/10.1186/s12885-015-1106-3>
- 921 45. Ryu H-H, Jung S, Jung T-Y, Moon K-S, Kim I-Y, Jeong Y-I, et al. Role of  
922 metallothionein 1E in the migration and invasion of human glioma cell lines. Int  
923 J Oncol [Internet]. 2012 Oct [cited 2019 Jul 23];41(4):1305–13. Available from:  
924 <https://www.spandidos-publications.com/10.3892/ijo.2012.1570>
- 925 46. Selvaraj N, Budka JA, Ferris MW, Plotnik JP, Hollenhorst PC. Extracellular  
926 signal-regulated kinase signaling regulates the opposing roles of JUN family  
927 transcription factors at ETS/AP-1 sites and in cell migration. Mol Cell Biol  
928 [Internet]. 2015 Jan 1 [cited 2019 Jul 23];35(1):88–100. Available from:  
929 <http://mcb.asm.org/lookup/doi/10.1128/MCB.00982-14>
- 930 47. Kake S, Usui T, Ohama T, Yamawaki H, Sato K. Death-associated protein  
931 kinase 3 controls the tumor progression of A549 cells through ERK MAPK/c-  
932 Myc signaling. Oncol Rep [Internet]. 2017 Feb [cited 2019 Jul 23];37(2):1100–  
933 6. Available from: [https://www.spandidos-](https://www.spandidos-publications.com/10.3892/or.2017.5359)  
934 [publications.com/10.3892/or.2017.5359](https://www.spandidos-publications.com/10.3892/or.2017.5359)
- 935 48. Lavigne MD, Vatsellas G, Polyzos A, Mantouvalou E, Sianidis G, Maraziotis I,  
936 et al. Composite macroH2A/NRF-1 Nucleosomes Suppress Noise and  
937 Generate Robustness in Gene Expression. Cell Rep [Internet]. 2015 May [cited  
938 2019 Jul 23];11(7):1090–101. Available from:

- 939 <https://linkinghub.elsevier.com/retrieve/pii/S221112471500409X>
- 940 49. Segal T, Salmon-Divon M, Gerlitz G. The Heterochromatin Landscape in  
941 Migrating Cells and the Importance of H3K27me3 for Associated  
942 Transcriptome Alterations. *Cells* [Internet]. 2018 Nov 9 [cited 2019 Jul  
943 23];7(11):205. Available from: <http://www.mdpi.com/2073-4409/7/11/205>
- 944 50. Yokoyama Y, Hieda M, Nishioka Y, Matsumoto A, Higashi S, Kimura H, et al.  
945 Cancer-associated upregulation of histone H3 lysine 9 trimethylation promotes  
946 cell motility in vitro and drives tumor formation in vivo. *Cancer Sci* [Internet].  
947 2013 Jul [cited 2019 Aug 7];104(7):889–95. Available from:  
948 <http://doi.wiley.com/10.1111/cas.12166>
- 949 51. Bernstein E, Muratore-Schroeder TL, Diaz RL, Chow JC, Changolkar LN,  
950 Shabanowitz J, et al. A phosphorylated subpopulation of the histone variant  
951 macroH2A1 is excluded from the inactive X chromosome and enriched during  
952 mitosis. *Proc Natl Acad Sci U S A* [Internet]. 2008 Feb 5 [cited 2019 Jul  
953 23];105(5):1533–8. Available from:  
954 <http://www.pnas.org/cgi/doi/10.1073/pnas.0711632105>
- 955 52. Dardenne E, Pierredon S, Driouch K, Gratadou L, Lacroix-Triki M, Espinoza  
956 MP, et al. Splicing switch of an epigenetic regulator by RNA helicases  
957 promotes tumor-cell invasiveness. *Nat Struct Mol Biol* [Internet]. 2012 Nov 30  
958 [cited 2019 Jul 23];19(11):1139–46. Available from:  
959 <http://www.nature.com/articles/nsmb.2390>
- 960 53. Kapoor A, Goldberg MS, Cumberland LK, Ratnakumar K, Segura MF, Emanuel  
961 PO, et al. The histone variant macroH2A suppresses melanoma progression  
962 through regulation of CDK8. 2011;468(7327):1105–9.
- 963 54. Borghesan M, Fusilli C, Rappa F, Panebianco C, Rizzo G, Oben JA, et al. DNA

- 964 Hypomethylation and Histone Variant macroH2A1 Synergistically Attenuate  
965 Chemotherapy-Induced Senescence to Promote Hepatocellular Carcinoma  
966 Progression. 2017;76(3):594–606.
- 967 55. Li F, Yi P, Pi J, Li L, Hui J, Wang F, et al. QKI5-mediated alternative splicing of  
968 the histone variant macroH2A1 regulates gastric carcinogenesis. *Oncotarget*  
969 [Internet]. 2016 May 31 [cited 2019 Jul 23];7(22):32821–34. Available from:  
970 <http://www.oncotarget.com/fulltext/8739>
- 971 56. Gibson BA, Zhang Y, Jiang H, Hussey KM, Shrimp JH, Lin H, et al. Chemical  
972 genetic discovery of PARP targets reveals a role for PARP-1 in transcription  
973 elongation. *Science (80- )* [Internet]. 2016 Jul 1 [cited 2019 Aug  
974 7];353(6294):45–50. Available from:  
975 <http://www.ncbi.nlm.nih.gov/pubmed/27256882>
- 976 57. Hnisz D, Abraham BJ, Lee TI, Lau A, Saint-André V, Sigova AA, et al. Super-  
977 Enhancers in the Control of Cell Identity and Disease. *Cell* [Internet]. 2013 Nov  
978 7 [cited 2019 Aug 6];155(4):934–47. Available from:  
979 <http://www.ncbi.nlm.nih.gov/pubmed/24119843>
- 980 58. Donati B, Lorenzini E, Ciarrocchi A. BRD4 and Cancer: going beyond  
981 transcriptional regulation. *Mol Cancer* [Internet]. 2018 Dec 22 [cited 2019 Aug  
982 6];17(1):164. Available from: [https://molecular-](https://molecular-cancer.biomedcentral.com/articles/10.1186/s12943-018-0915-9)  
983 [cancer.biomedcentral.com/articles/10.1186/s12943-018-0915-9](https://molecular-cancer.biomedcentral.com/articles/10.1186/s12943-018-0915-9)
- 984 59. He Y, Long W, Liu Q. Targeting Super-Enhancers as a Therapeutic Strategy  
985 for Cancer Treatment. *Front Pharmacol* [Internet]. 2019 Apr 11 [cited 2019 Aug  
986 6];10:361. Available from: <http://www.ncbi.nlm.nih.gov/pubmed/31105558>
- 987 60. Yang P-C, Liu Z-Q, Mahmood T. Western blot: Technique, theory and trouble  
988 shooting. *N Am J Med Sci* [Internet]. 2014 [cited 2019 Jul 23];6(3):160.

- 989 Available from: <http://www.najms.org/text.asp?2014/6/3/160/128482>
- 990 61. Rao X, Huang X, Zhou Z, Lin X. An improvement of the 2<sup>-delta delta CT</sup>
- 991 method for quantitative real-time polymerase chain reaction data analysis.
- 992 *Biostat Bioinforma Biomath* [Internet]. 2013 Aug [cited 2019 Jul 23];3(3):71–85.
- 993 Available from: <http://www.ncbi.nlm.nih.gov/pubmed/25558171>
- 994 62. Tolza C, Bejjani F, Evanno E, Mahfoud S, Moquet-Torcy G, Gostan T, et al.
- 995 AP-1 Signaling by Fra-1 Directly Regulates HMGA1 Oncogene Transcription in
- 996 Triple-Negative Breast Cancers. *Mol Cancer Res* [Internet]. 2019 Oct [cited
- 997 2019 Oct 29];17(10):1999–2014. Available from:
- 998 <http://mcr.aacrjournals.org/lookup/doi/10.1158/1541-7786.MCR-19-0036>
- 999 63. Chan HL, Beckedorff F, Zhang Y, Garcia-Huidobro J, Jiang H, Colaprico A, et
- 1000 al. Polycomb complexes associate with enhancers and promote oncogenic
- 1001 transcriptional programs in cancer through multiple mechanisms. *Nat Commun*
- 1002 [Internet]. 2018 [cited 2019 Aug 7];9(1):3377. Available from:
- 1003 <http://www.ncbi.nlm.nih.gov/pubmed/30139998>
- 1004 64. Dobin A, Davis CA, Schlesinger F, Drenkow J, Zaleski C, Jha S, et al. STAR:
- 1005 ultrafast universal RNA-seq aligner. *Bioinformatics* [Internet]. 2013 Jan 1 [cited
- 1006 2019 Jul 23];29(1):15–21. Available from:
- 1007 [https://academic.oup.com/bioinformatics/article-](https://academic.oup.com/bioinformatics/article-lookup/doi/10.1093/bioinformatics/bts635)
- 1008 [lookup/doi/10.1093/bioinformatics/bts635](https://academic.oup.com/bioinformatics/article-lookup/doi/10.1093/bioinformatics/bts635)
- 1009 65. Li H, Handsaker B, Wysoker A, Fennell T, Ruan J, Homer N, et al. The
- 1010 Sequence Alignment/Map format and SAMtools. *Bioinformatics* [Internet]. 2009
- 1011 Aug 15 [cited 2019 Jul 23];25(16):2078–9. Available from:
- 1012 <http://www.ncbi.nlm.nih.gov/pubmed/19505943>
- 1013 66. Ram F, Ryan DP, Bhardwaj V, Kilpert F, Richter AS, Heyne S, et al.

- 1014 deepTools2 : a next generation web server for deep-sequencing data analysis.  
1015 2016;44(April):160–5.
- 1016 67. Helmuth J CH. normr: Normalization and difference calling in ChIP-seq data . R  
1017 Packag version 180, <https://github.com/your-highness/normR>. 2018;2018.
- 1018 68. James T. Robinson, Helga Thorvaldsdóttir, Wendy Winckler, Mitchell Guttman,  
1019 Eric S. Lander, Gad Getz JPM. Integrative genomics viewer. Nat Biotechnol.  
1020 2000;29(220):23–4.
- 1021 69. Thorvaldsdóttir H, Robinson JT, Mesirov JP. Integrative Genomics Viewer  
1022 (IGV): high-performance genomics data visualization and exploration. Brief  
1023 Bioinform [Internet]. 2013 Mar 1 [cited 2019 Jul 23];14(2):178–92. Available  
1024 from: <https://academic.oup.com/bib/article-lookup/doi/10.1093/bib/bbs017>
- 1025 70. H. Wickham. ggplot2: Elegant Graphics for Data Analysis. Springer-Verlag  
1026 New York [Internet]. 2016;174(1):245–6. Available from:  
1027 [http://doi.wiley.com/10.1111/j.1467-985X.2010.00676\\_9.x](http://doi.wiley.com/10.1111/j.1467-985X.2010.00676_9.x)
- 1028 71. Yu G, Wang L-G, He Q-Y. ChIPseeker: an R/Bioconductor package for ChIP  
1029 peak annotation, comparison and visualization. Bioinformatics [Internet]. 2015  
1030 Jul 15 [cited 2019 Jul 23];31(14):2382–3. Available from:  
1031 [https://academic.oup.com/bioinformatics/article-](https://academic.oup.com/bioinformatics/article-lookup/doi/10.1093/bioinformatics/btv145)  
1032 [lookup/doi/10.1093/bioinformatics/btv145](https://academic.oup.com/bioinformatics/article-lookup/doi/10.1093/bioinformatics/btv145)
- 1033 72. Blinka S, Reimer MH, Pulakanti K, Pinello L, Yuan G-C, Rao S. Identification of  
1034 Transcribed Enhancers by Genome-Wide Chromatin Immunoprecipitation  
1035 Sequencing. Methods Mol Biol [Internet]. 2017 [cited 2019 Jul 23];1468:91–  
1036 109. Available from: <http://www.ncbi.nlm.nih.gov/pubmed/27662872>
- 1037 73. Zhang X, Chiang H-C, Wang Y, Zhang C, Smith S, Zhao X, et al. Attenuation of  
1038 RNA polymerase II pausing mitigates BRCA1-associated R-loop accumulation

- 1039 and tumorigenesis. *Nat Commun* [Internet]. 2017 Aug 26 [cited 2019 Jul  
1040 23];8(1):15908. Available from: <http://www.ncbi.nlm.nih.gov/pubmed/28649985>
- 1041 74. Stempor P, Ahringer J. SeqPlots - Interactive software for exploratory data  
1042 analyses, pattern discovery and visualization in genomics. *Wellcome Open*  
1043 *Res* [Internet]. 2016;1(0):14. Available from:  
1044 <https://wellcomeopenresearch.org/articles/1-14/v1>
- 1045 75. Love MI, Huber W, Anders S. Moderated estimation of fold change and  
1046 dispersion for RNA-seq data with DESeq2. *Genome Biol* [Internet]. 2014 Dec 5  
1047 [cited 2019 Jul 23];15(12):550. Available from:  
1048 <http://genomebiology.biomedcentral.com/articles/10.1186/s13059-014-0550-8>
- 1049 76. K B. EnhancedVolcano: Publication-ready volcano plots with enhanced  
1050 colouring and labeling . <https://github.com/kevinblighe/EnhancedVolcano>  
1051 [Internet]. 2018;R package:2018. Available from:  
1052 <https://github.com/kevinblighe/EnhancedVolcano>.
- 1053 77. Ritchie ME, Phipson B, Wu D, Hu Y, Law CW, Shi W, et al. Limma powers  
1054 differential expression analyses for RNA-sequencing and microarray studies.  
1055 *Nucleic Acids Res*. 2015;43(7):e47.
- 1056 78. Durinck S, Moreau Y, Kasprzyk A, Davis S, De Moor B, Brazma A, et al.  
1057 BioMart and Bioconductor: a powerful link between biological databases and  
1058 microarray data analysis. *Bioinformatics* [Internet]. 2005 Aug 15 [cited 2019 Jul  
1059 23];21(16):3439–40. Available from:  
1060 [https://academic.oup.com/bioinformatics/article-](https://academic.oup.com/bioinformatics/article-lookup/doi/10.1093/bioinformatics/bti525)  
1061 [lookup/doi/10.1093/bioinformatics/bti525](https://academic.oup.com/bioinformatics/article-lookup/doi/10.1093/bioinformatics/bti525)
- 1062 79. Durinck S, Spellman PT, Birney E, Huber W. Mapping identifiers for the  
1063 integration of genomic datasets with the R/Bioconductor package biomaRt. *Nat*

1064 Protoc [Internet]. 2009 Aug 23 [cited 2019 Jul 23];4(8):1184–91. Available  
1065 from: <http://www.nature.com/articles/nprot.2009.97>  
1066 80. Caroline A Schneider WSR& KWE. NIH Image to ImageJ: 25 years of image  
1067 analysis. INMATEH - Agric Eng [Internet]. 2012;9(7):671–5. Available from:  
1068 <http://dx.doi.org/10.1038/nmeth.2089>

1069

## 1070 **Figure legends**

1071

1072 **Fig 1. Histone mH2A1 isoforms are incorporated to “facultative-like”**  
1073 **heterochromatin.** (A) Overlap of “mH2A1.1” (Ab  $\alpha$ mH2A1.1) peaks with “mH2A1”  
1074 (Ab  $\alpha$ mH2A1). Peaks detected exclusively by Ab  $\alpha$ mH2A1.1 are called “mH2A1.1  
1075 only”, peaks detected exclusively by Ab  $\alpha$ mH2A1 are called “mH2A1.2 only” and  
1076 peaks detected by both correspond to mH2A1.1 only or mH2A1.1 and mH2A1.2 in  
1077 unknown proportions, called “mH2A1s”. (B) Proportions of mH2A1 isoforms peaks at  
1078 different genomic features (Methods). Arrows highlights differences between the two  
1079 ChIP-seq. Promoters are defined around TSS. (C) Overlap of heterochromatin  
1080 histone marks (H3K27me3 and H3K9me3) with mH2A1.1 peaks (left) and mH2A1  
1081 peaks (right). Percentages of overlaps are also given. Results of fisher exact tests  
1082 are shown (p-value (p) and Odd ratio) (Methods). (D) Genome browser view of ChIP-  
1083 seq profiles illustrating occupancy of mH2A1 isoforms with heterochromatin histone  
1084 marks (H3K27me3 and H3K9me3). At the top, region with high level of H3K27me3  
1085 and at the bottom, region with high level of H3K9me3. Peaks and unstranded RNA-  
1086 seq signal are shown in parallel. The black arrows show the direction of transcription.  
1087 (E) Heatmap showing enrichment of mH2A1 isoforms sites (see Fig 1A) with  
1088 H3K27me3 ; from left to right, 5 equal size categories as a function of differences in

1089 H3K27me3 and H3K9me3 signals. Stars indicate significance, red and blue  
1090 highlights positive and negative correlations, respectively.

1091

1092 **Fig 2. The mH2A1.1 isoform is enriched at super-enhancers.** (A) Genome  
1093 browser view of ChIP-seq profiles illustrating occupancy of mH2A1 isoforms with  
1094 H3K27ac and H3K4me1 histone marks on genomic regions excluding TSS. (B)  
1095 Overlap of “putative” enhancers (Methods) with mH2A1 isoforms. (C) Genome  
1096 browser view of ChIP-seq profiles illustrating occupancy of mH2A1 isoforms (Ab  
1097  $\alpha$ mH2A1.1 and Ab  $\alpha$ mH2A1) at “putative” super-enhancers (SEs). SEs were defined  
1098 using the ROSE package (Methods). (D) Overlap of SEs with mH2A1 isoforms. On  
1099 genome browser views, peaks and unstranded RNA-seq signal are shown in parallel.  
1100 The black arrows show the direction of transcription. On venn diagrams, percentages  
1101 of overlaps are given. Results of fisher exact tests are shown (p-value (p) and Odd  
1102 ratio) (see Materials and Methods).

1103

1104 **Fig 3. mH2A1.1 is recruited to the transcription start site of active genes.** (A)  
1105 Overlap of mH2A1 isoforms with TSSs (+/- 1kb). (B) Metagene plot of average (+/-  
1106 s.d) of mH2A1 isoforms enrichment at TSSs (+/- 2 kb) categorized by gene  
1107 expression levels (Methods). Colors denote gene classes as indicated. (C) Genome  
1108 browser view of ChIP-seq profiles illustrating the binding of mH2A1.1 to the TSS of a  
1109 transcribed gene in an open chromatin state. Peaks and unstranded RNA-seq signal  
1110 are shown in parallel. The black arrows show the direction of transcription. (D)  
1111 Heatmap showing peak enrichment of mH2A1 isoforms sites (see Fig 1A) at TSSs  
1112 (+/- 1kb), divided into 5 equal size categories as a function of expression level  
1113 (Methods). Stars indicate significance. Red and blue highlights positive and negative

1114 correlations, respectively.(E) Metagene plot of average (+/- s.d) of mH2A1.1,  
1115 H3K27ac and PolII enrichment at TSS (+/- 2kb). (F) Overlap of mH2A1 isoforms with  
1116 Pol II at TSSs. On venn diagrams, percentages of overlaps are given. Results of  
1117 fisher exact tests are shown (p-value (p) and Odd ratio) (see Materials and Methods).  
1118

1119 **Fig 4. mH2A1.1 activates gene expression when it binds only on their TSSs.** (A)  
1120 Volcano plot showing fold change of gene expression in mH2A1.1 KD compared to  
1121 WT MDA-MB231 cells. Red dots represent significantly de-regulated genes with a  
1122 foldchange > 1.5 and padj < 0.1. Total mH2A1.1 regulated-genes are shown. (B)  
1123 Heatmap showing mH2A1 isoforms and Pol II relative enrichment around the TSS  
1124 (+/- 10 kb) of mH2A1.1 KD de-regulated genes (see Fig 4A). Colour intensity reflects  
1125 level of ChIP-seq enrichment. (C) Genome browser view of ChIP-seq profiles  
1126 illustrating mH2A1.1 localization and genomic environment of a mH2A1.1 repressed-  
1127 gene. (D) As in (C) but for a mH2A1.1 activated- gene. On genome browser views,  
1128 peaks and unstranded RNA-seq signal are shown in parallel. The black arrows show  
1129 the direction of transcription.

1130

1131 **Fig 5. mH2A1.1 binds a subset of TSSs of paused genes and promotes their**  
1132 **transcription.** (A) Heatmap showing Pol II and mH2A1 isoforms enrichment around  
1133 the TSS (+/- 10 kb) of transcribed genes (n=10,198) ranked by their pausing index  
1134 (Methods). Colour intensity reflects level of ChIP-seq enrichment. (B) Heatmap  
1135 showing correlation between mH2A1.1 peak width at TSSs (+/-1 kb) and pausing  
1136 index. Genes were divided in 3 equal size categories according to their pausing  
1137 index. mH2A1.1 peaks were divided in 5 categories according to their width. Stars  
1138 indicate significance. Red and blue highlights positive and negative correlations,

1139 respectively. (C) Genome browser view of ChIP-seq profiles illustrating mH2A1.1  
1140 localization on a paused gene. Peaks and unstranded RNA-seq signal are shown in  
1141 parallel. The black arrows show the direction of transcription. (D) Overlap of mH2A1  
1142 isoforms sites (mH2A1.1 only and mH2A1.2 only, see Fig 1A) with paused genes  
1143 (Pausing index , PI > 2, n=6,821) at their TSSs. (E) Overlap of mH2A1.1 regulated-  
1144 genes with paused genes (PI > 2, n=6,821). (F) Boxplot showing pausing index of  
1145 five different groups of genes, as indicated. “\*\*\*\*” = p-value < 2.2x10<sup>-16</sup>. NS, not  
1146 significant. On venn diagrams, percentages of overlaps are given. Results of fisher  
1147 exact tests are shown (p-value (p) and Odd ratio) (see Materials and Methods).

1148

1149 **Fig 6. mH2A1.1 inhibits cell migration by in part favouring expression of**  
1150 **paused genes involved in cytoskeleton and cell adhesion in MDA-MB231 cells.**

1151 (A) Representative DIC microscopy images of WT, mH2A1.1 KD (two different  
1152 siRNA) and mH2A1.2 KD MDA-MB231 cells. Scale bar = 100 μM. (B)  
1153 Immunofluorescence of Actin (up), Tubulin-α (middle) and Vimentin (down) in WT,  
1154 mH2A1.1 KD and mH2A1.2 KD MDA-MB231 cells. Nuclei are stained with Hoechst.  
1155 Scale bar = 20 μM. (C) Boyden chamber assay representatives images of WT,  
1156 mH2A1.1 KD and mH2A1.2 KD MDA-MB231 cells. Only migrated cells are labelled in  
1157 purple. Scale bar = 150 μM. (D) Quantification of Boyden chamber assay presented  
1158 in (C). Error bar represents s.d from n=3 independent experiments as illustrated in  
1159 (C). “\*” = p-value (p) < 0.05, \*\*, p < 0.01. (E) Overlap of paused genes (n= 6,821)  
1160 with mH2A1.1 regulated genes related to cytoskeleton and cell adhesion (see  
1161 Materials and Methods). On venn diagrams, percentages of overlaps are given.  
1162 Results of fisher exact tests are shown (p-value (p) and Odd ratio) (see Materials and  
1163 Methods).

1164

1165 **S1 Fig. The antibody Ab  $\alpha$ H2A1.1 recognizes unequivocally only the isoform**  
1166 **mH2A1.1.** (A) RTqPCR on MDA-MB231 and MCF7 cells showing their relative  
1167 mH2A1 isoforms mRNA expression level. Relative expressions are normalized by  
1168 RPLP0 mRNA. (B) Western blot on whole cell extracts of MDA-MB231 and MCF7  
1169 cells showing the better affinity of Ab  $\alpha$ H2A1.1 to recognize mH2A1.1 compared to  
1170 Ab#37264 (Ab  $\alpha$ H2A1). Ab#61427 is specific to mH2A1.2. GAPDH is used as a  
1171 loading control. (C) Western blot showing specific recognition of mH2A1.1 isoform by  
1172 Ab  $\alpha$ H2A1.1 antibody. For that, HEK-293T cells were transfected with plasmids  
1173 coding for Flag-mH2A1.1 (Flag1.1) or Flag-mH2A1.2 (Flag1.2) fusion overexpressed-  
1174 protein. Western blot was then done with Ab  $\alpha$ H2A1.1, Ab#Flag and Ab#E215 (that  
1175 preferentially recognizes mH2A1.2) antibodies on whole cell extracts. GAPDH is  
1176 used as a loading control. (D) Immunofluorescence in HEK-293T cells showing  
1177 specific recognition of mH2A1.1 isoform by Ab  $\alpha$ H2A1.1. (E) Western blot on ChIP  
1178 extracts from HEK-293T cells overexpressing Flag1.1 or Flag1.2 showing that Ab  
1179  $\alpha$ H2A1.1 immunoprecipitates only mH2A1.1 isoform (Methods). Different extracts  
1180 were loaded : Input fraction (Input), Non immunoprecipitated fraction (NoIP) and  
1181 immunoprecipitated fraction (IP). Percentages represent percentages loaded on  
1182 western blot compared to quantity used for ChIP. (F) Western blot showing that Ab  
1183  $\alpha$ H2A1.1 is also working in ChIP in MDA-MB231 cells on the endogenous protein.  
1184 (G) As in (C), but for Ab  $\alpha$ H2A1 (Ab#37264) antibody showing that its antibody  
1185 recognizes both isoforms but it less affine for Flag1.1 than Ab  $\alpha$ H2A1.1. (H) As in  
1186 (G), but in immunofluorescence. (I), As in (E), but for Ab  $\alpha$ H2A1 (Ab#37264)  
1187 antibody.

1188 **S2 Fig.** (A) Whole genome spearman correlation heatmap of ChIP-seq data.  
1189 Pearson coefficient correlations (PCC,  $r$ ) are given. Red and blue colours denote  
1190 high correlation ( $r$  close to 1) and anti-correlation ( $r$  close to -1), respectively. (B)  
1191 Table showing PCCs obtained between mH2A1.1 and mH2A1 at different genomic  
1192 region, as presented.

1193 **S3 Fig. Specific partial depletion of mH2A1 isoforms in MDA-MB231 cells.** (A)  
1194 RTqPCR showing specific partial depletion of mH2A1 isoforms mRNA by specific  
1195 siRNA three days post-transfection (see Materials and Methods). (B) Western blot  
1196 showing specific depletion of mH2A1 isoforms protein by specific siRNA three days  
1197 post-transfection. H3 is used as a loading control. (C) Immunofluorescence showing  
1198 specific partial depletion of mH2A1 isoforms by specific siRNA three days post-  
1199 transfection. DNA is labelled with Hoechst. Scale bar = 10  $\mu$ m. (D) As in (A) but with  
1200 a second siRNA against mH2A1.1. (E) As in (B) but with a second siRNA against  
1201 mH2A1.1. GAPDH is used as a loading control. (F) RTqPCR analysis of a subset of  
1202 RNAseq-defined mH2A1.1 regulated-genes. Genes are divided in three groups, as  
1203 indicated. On RTqPCR, mRNA expressions are relatives to WT condition and  
1204 normalized by RPLP0 mRNA. Error bars represent s.d from independent  
1205 experiments ( $n \geq 2$ ). “\*” :  $p < 0.05$ , “\*\*\*” :  $p < 0.001$ , NS, not significant. On western  
1206 blot, mH2A1.1 and mH2A1.2 proteins are detected with Ab  $\alpha$ mH2A1.1 and  
1207 Ab#61427, respectively. Quantifications are showed, normalized by protein loading  
1208 control.

1209 **S4 Fig.** (A) mH2A1 and mH2A1.1 binding at genomic regions selected based on  
1210 ChIP-sequencing. Localisation of primers used for ChIP-qPCR are shown in red. (B)  
1211 Occupancy of mH2A1 isoforms (left part : Ab  $\alpha$ mH2A1.1 ; right part : Ab  $\alpha$ mH2A1)  
1212 analysed by ChIP-qPCR in control cells (WT) and cells partially deficient for

1213 mH2A1.1 using two different siRNA (mH2A1.1 KD #1 and mH2A1.1 KD #2). Error  
1214 bars represent +s.d from independent experiments (n>=2).

1215 **S5 Fig. Levels of H3K27me3 and H3K9me3 are anti-correlated on common**  
1216 **H3K27me3/H3K9me3 peaks.** (A) Boxplots showing H3K27me3 and H3K9me3  
1217 enrichment levels on H3K27me3/H3K9me3 common peaks. Peaks were divided into  
1218 5 equal size categories according to the level of H3K27me3, as mentioned. (B)  
1219 Histogram showing proportions of heterochromatin genomic localization, as  
1220 mentioned. Peaks were divided into 5 equal size categories according to ratio  
1221 between H3K27me3 and H3K9me3, as mentioned.

1222 **S6 Fig. The mH2A1.1 isoform binds to TSSs in open chromatin state whereas**  
1223 **mH2A1.2 binds to TSSs in closed chromatin state.** (A) TSS (+/- 1kb) centred  
1224 spearman correlation heatmap of ChIP-seq data. Pearson coefficient correlations  
1225 (PCC, r) are given. Red and blue colours denote high correlation (r close to 1) and  
1226 anti-correlation (r close to -1), respectively. (B) Overlap of mH2A1 isoforms sites  
1227 (mH2A1.1 only and mH2A1.2 only, see Fig. 1a) with H3K4me3 and Pol II at TSS (+/-  
1228 1 kb). (C) As in (B), but with H3K9me3 and H3K27me3 histone marks. Results of  
1229 fisher exact tests are shown (p-value (p) and Odd ratio) (see Materials and Methods).

1230 **S7 Fig. The mH2A1.1 isoform binds the TSSs of transcribed genes.** (A) Boxplots  
1231 of mH2A1 isoforms levels and Pol II at TSS (+/- 1kb) categorized by gene expression  
1232 levels (see Materials and Methods). Colors denote gene classes, as indicated. “\*\*\*\*”  
1233 p-value < 2.2x10<sup>-16</sup> (see Materials and Methods). (B) Metagene plot of average (+/-  
1234 s.d) of mH2A1 isoforms enrichment from TSS to TES (+/- 2 kb) categorized by gene  
1235 expression levels (Methods). Colors denote gene classes, as indicated. (C) Genome  
1236 browser view of ChIP-seq profiles illustrating occupancy of mH2A1 isoforms on a not  
1237 expressed gene. (D) As in (C) but for a highly expressed gene. (E) Heatmap showing

1238 peak enrichment of Pol II and histone marks at TSS (+/- 1kb) divided into 5 equal  
1239 size categories as a function of expression level (Methods). Stars indicate  
1240 significance. Red highlights positive and blue indicates negative correlations. (F)  
1241 TSS-centred spearman correlation heatmap of ChIP-seq data. Pearson coefficient  
1242 correlations (PCC, r) are given. Red and blue colours denote high correlation (r close  
1243 to 1) and anti-correlation (r close to -1), respectively. On genome browser views,  
1244 peaks and unstranded RNA-seq signal are shown in parallel. The black arrows show  
1245 the direction of transcription.

1246

1247 **S8 Fig. The mH2A1.1 isoform regulates expression of active genes.** (A) Boxplot  
1248 comparing gene expression of three groups of genes (as indicated) between WT and  
1249 mH2A1.1 KD cells. (B) Pie chart showing proportion of mH2A1.1 regulated-genes  
1250 categorized by gene expression levels in WT cells (see Materials and Methods).  
1251 Colors denote gene classes, as indicated. Results of fisher exact tests are shown (p-  
1252 value (p) and Odd ratio) (see Materials and Methods). (C) Boxplot showing mH2A1  
1253 isoforms occupancy levels, Pol II and histone marks at TSS on mH2A1.1 KD  
1254 regulated genes and not affected genes, as indicated. On boxplots, p-value are  
1255 shown, “\*\*\*\*” = p-value <  $2.2 \times 10^{-16}$ ; NS, not significant (see Materials and Methods).

1256

1257 **S9 Fig. The recruitment of mH2A1.1 differs between mH2A1.1-activated and**  
1258 **repressed genes.** (A) Metagene plot of average (+/- sd) of mH2A1 isoforms levels  
1259 and Pol II from TSS to TES (+/- 2 kb) on mH2A1.1 regulated-genes. (B) Heatmap  
1260 showing correlation between Pol II peak width at TSS (+/-1 kb) and pausing index.  
1261 Genes were divided in 3 equal size categories according to their pausing index. Pol II

1262 peaks were divided in 5 categories according to their width. Stars indicate  
1263 significance. Red and blue highlights positive and negative correlations, respectively.

1264

1265 **S10 Fig. The isoform mH2A1.1 modulates expression of genes involved in cell**  
1266 **cycle, DNA repair and cell shape.** (A) List of gene ontology (GO) terms for  
1267 mH2A1.1 activated-genes. The most significantly regulated ontologies were  
1268 determined by adjusted p-value and are shown in three different classes, Biological  
1269 Process (upper graph), Molecular function (middle graph) and Cellular Component  
1270 (lower graph). A full list of enriched GO terms is provided in S4 Table. (B) As in (A)  
1271 but for mH2A1.1 repressed-genes.

1272

## 1273 **Supporting information legends**

1274

1275 S1 Table. List of antibodies used for western blot, immunofluorescence, and ChIP.

1276 S2 Table. Summary of ChIP-seq and RNA-seq.

1277 S3 Table. List of mH2A1.1-regulated genes.

1278 S4 Table. List of GO terms related to mH2A1.1-regulated genes.

1279 S5 Table. Sequences used for mH2A1.1 specific antibody production and siRNAs.

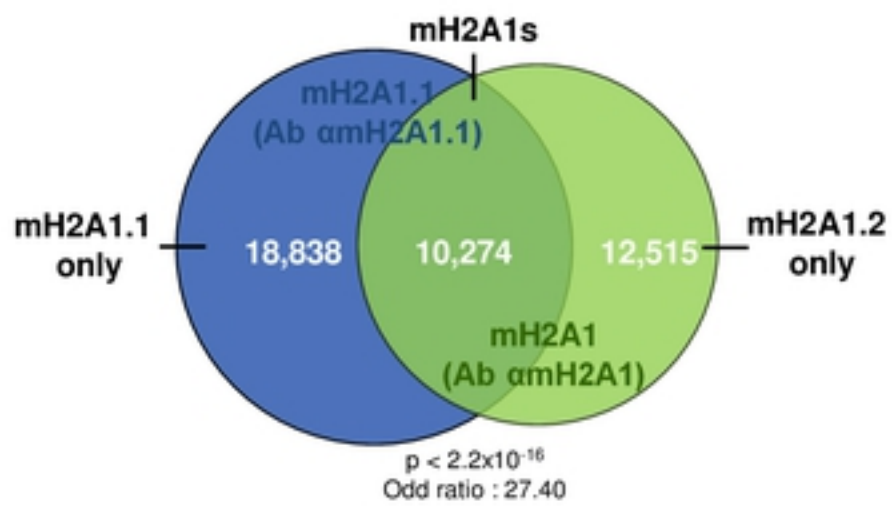
1280 S6 Table. List of primers used for RTqPCR.

1281 S7 Table. List of ChIPqPCR primers used for ChIPqPCR.

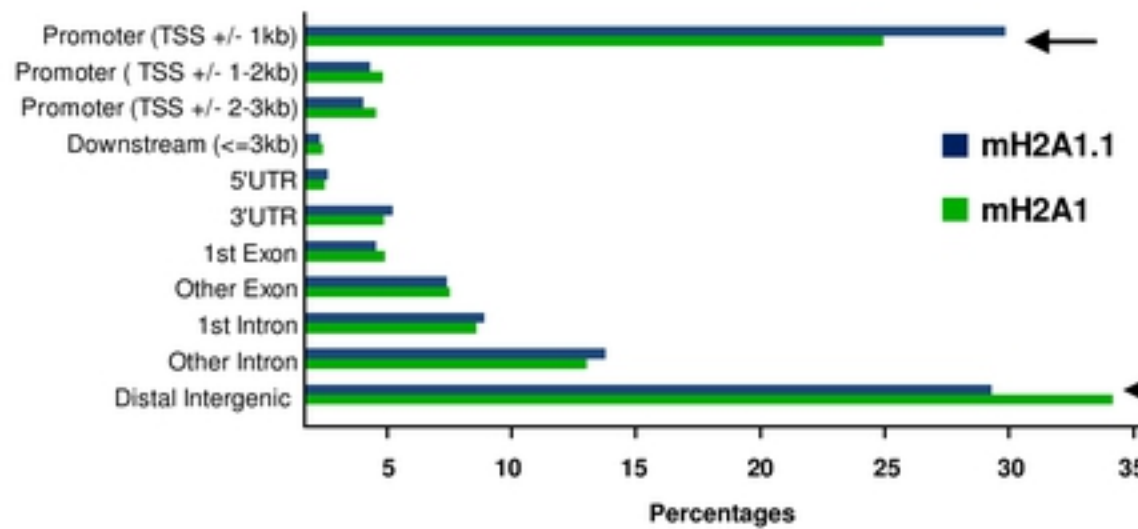
1282

**Fig 1**

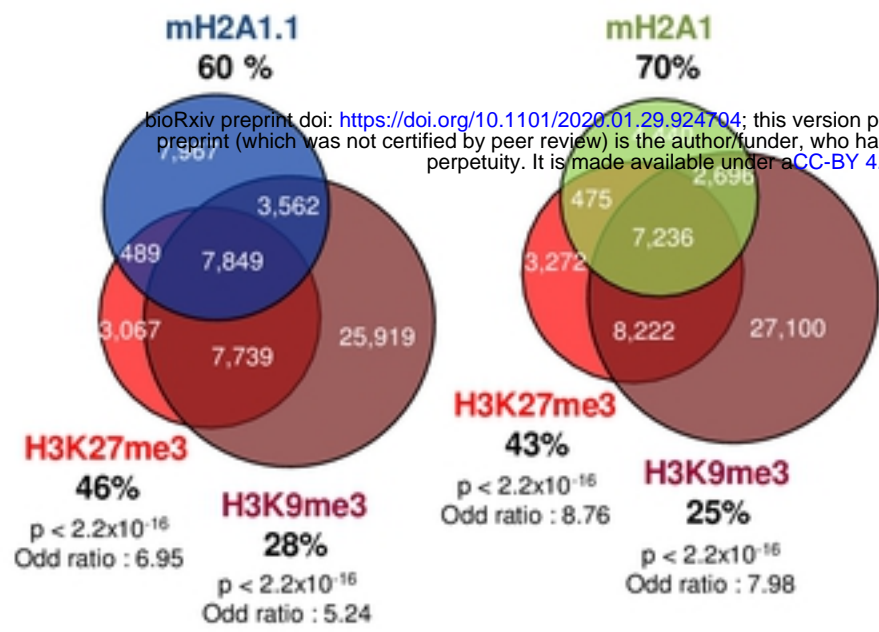
**A**



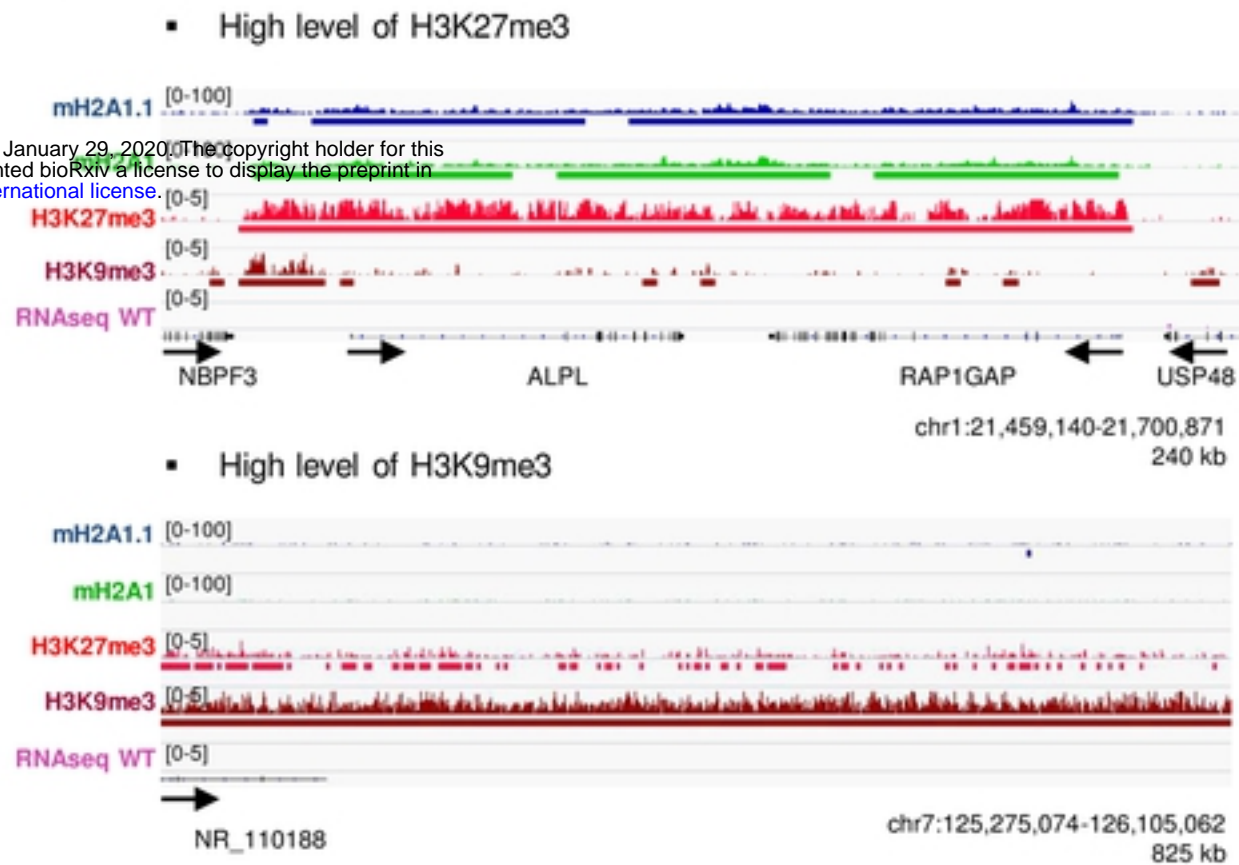
**B**



**C**



**D**



**E**

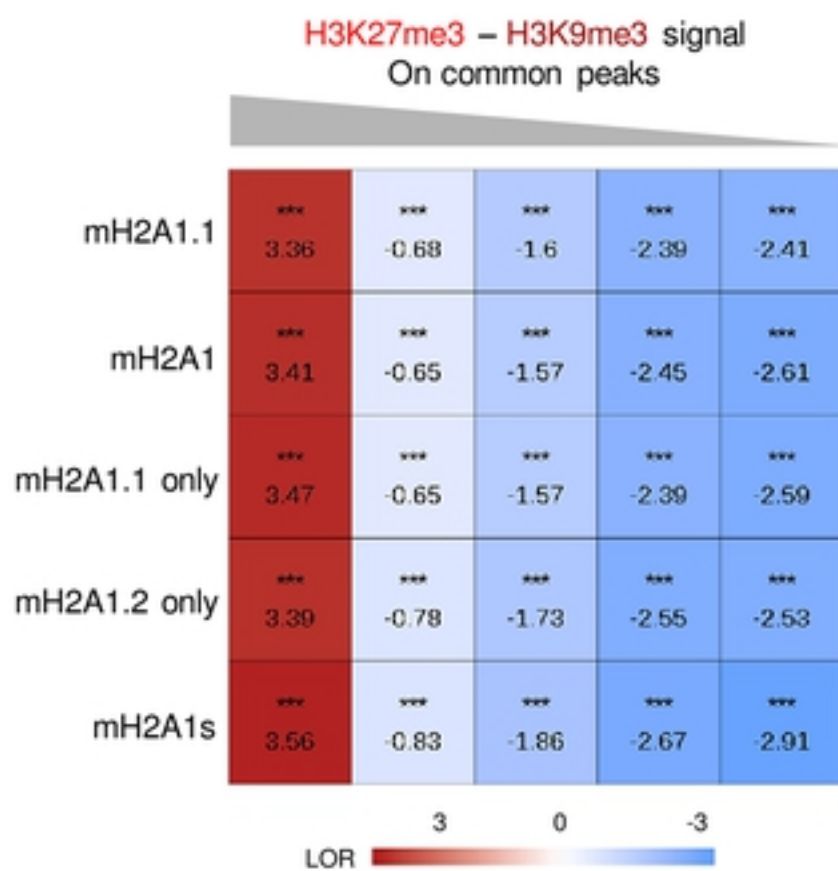
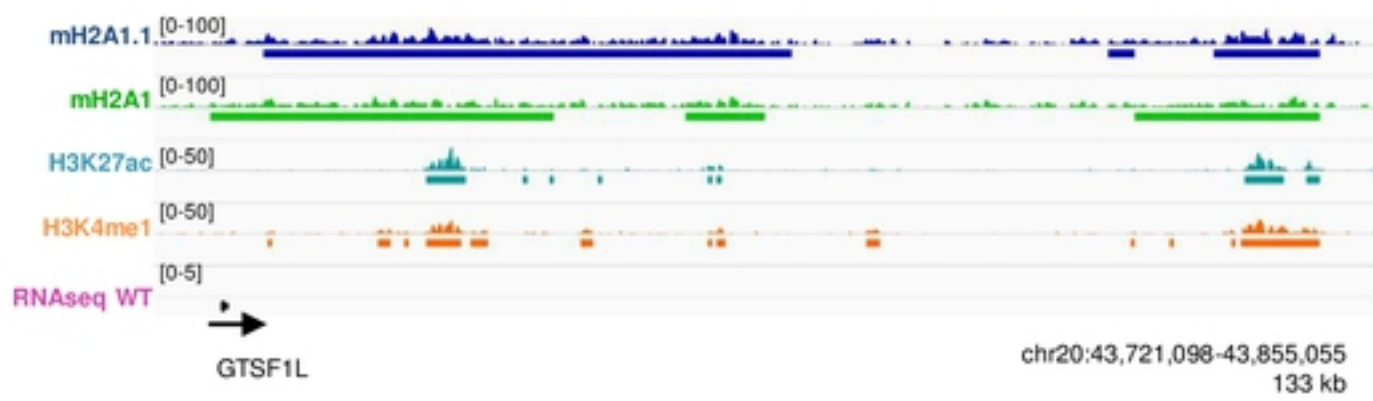
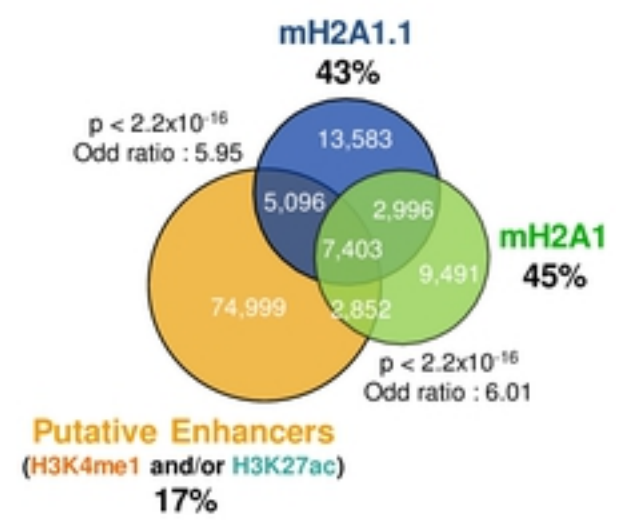


**Fig 2**

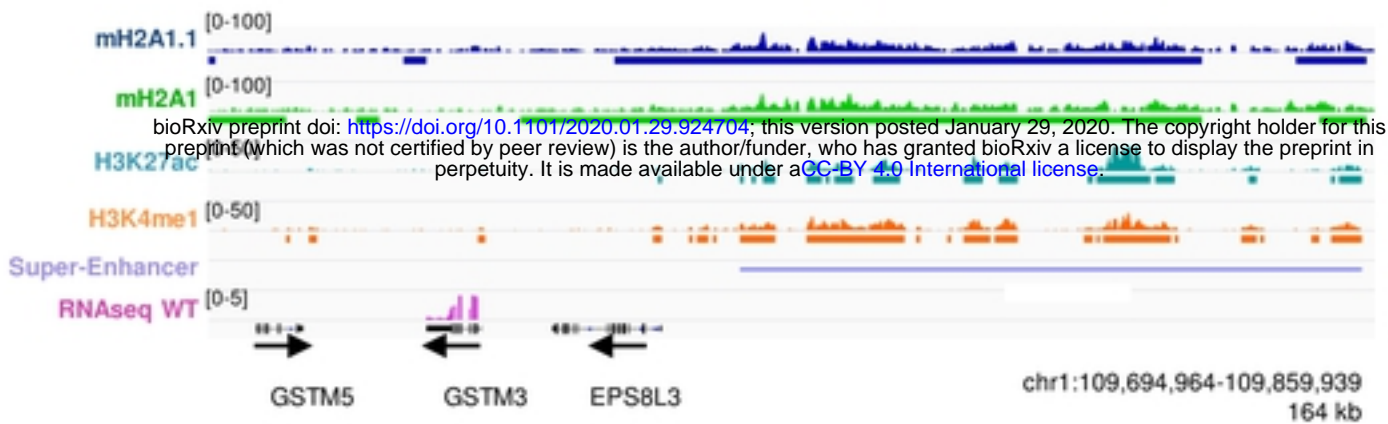
**A**



**B**



**C**



**D**

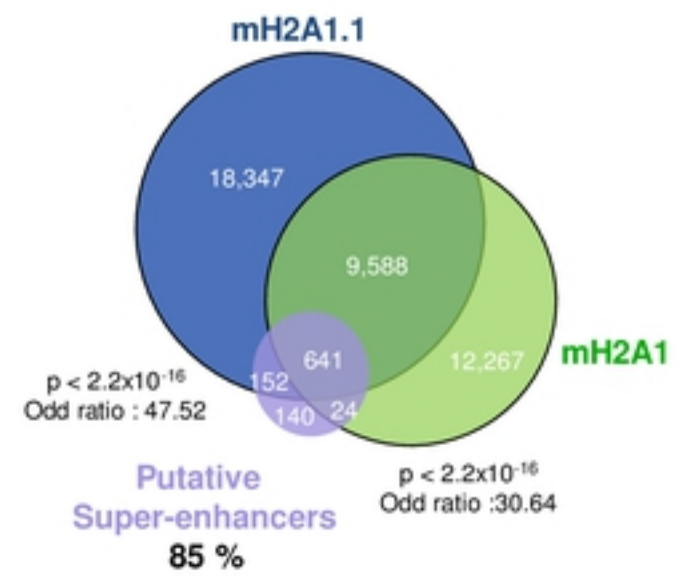
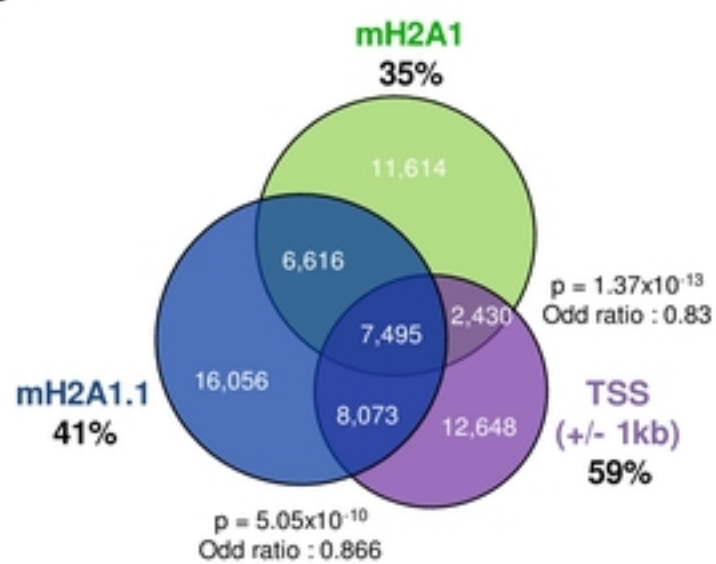
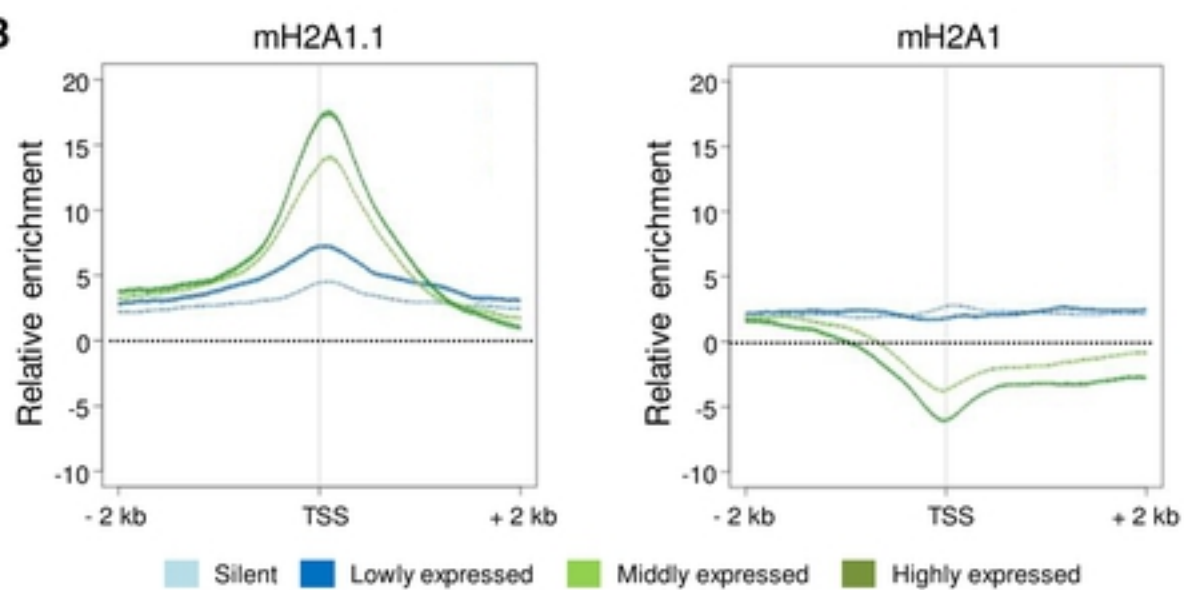


**Fig 3**

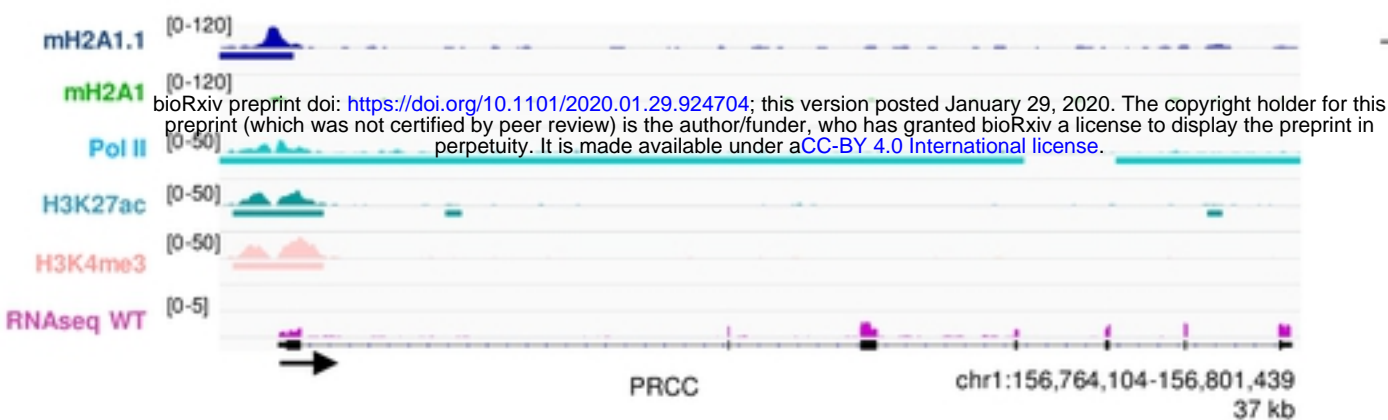
**A**



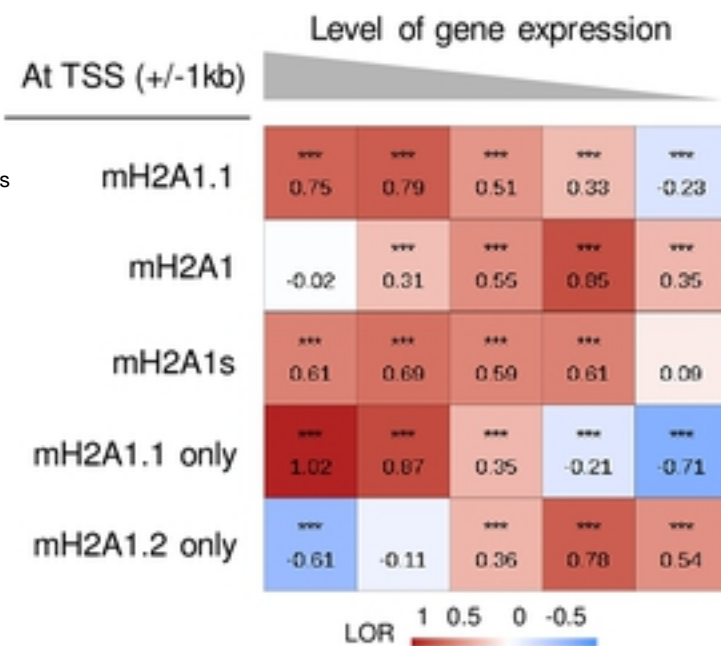
**B**



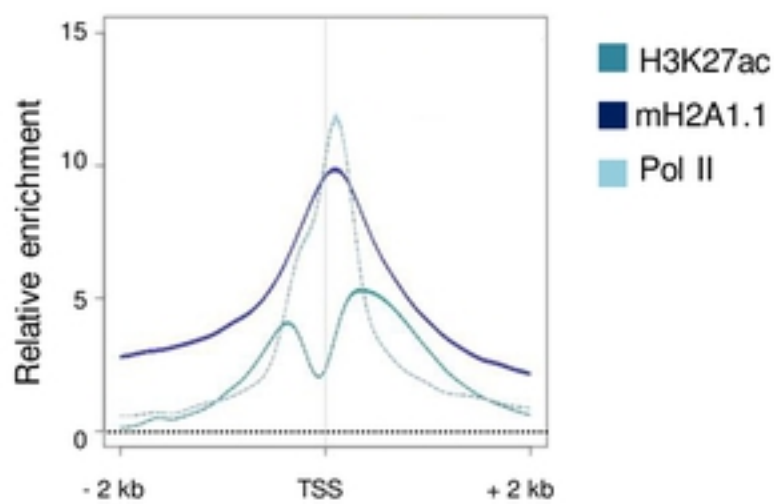
**C**



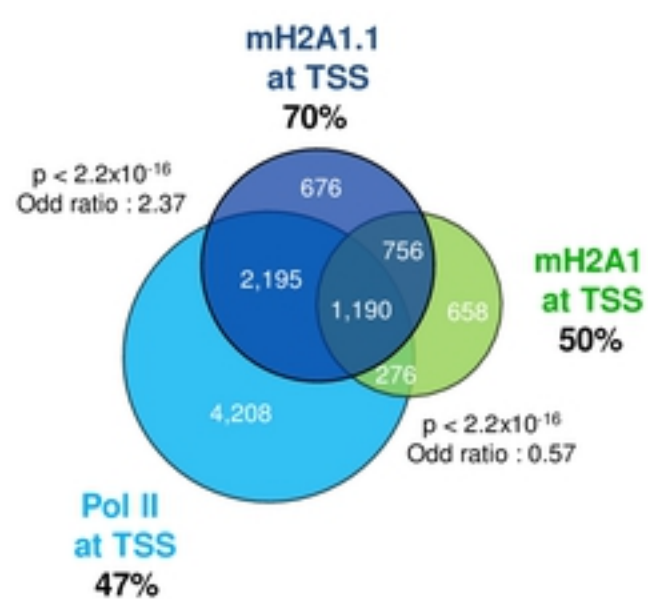
**D**

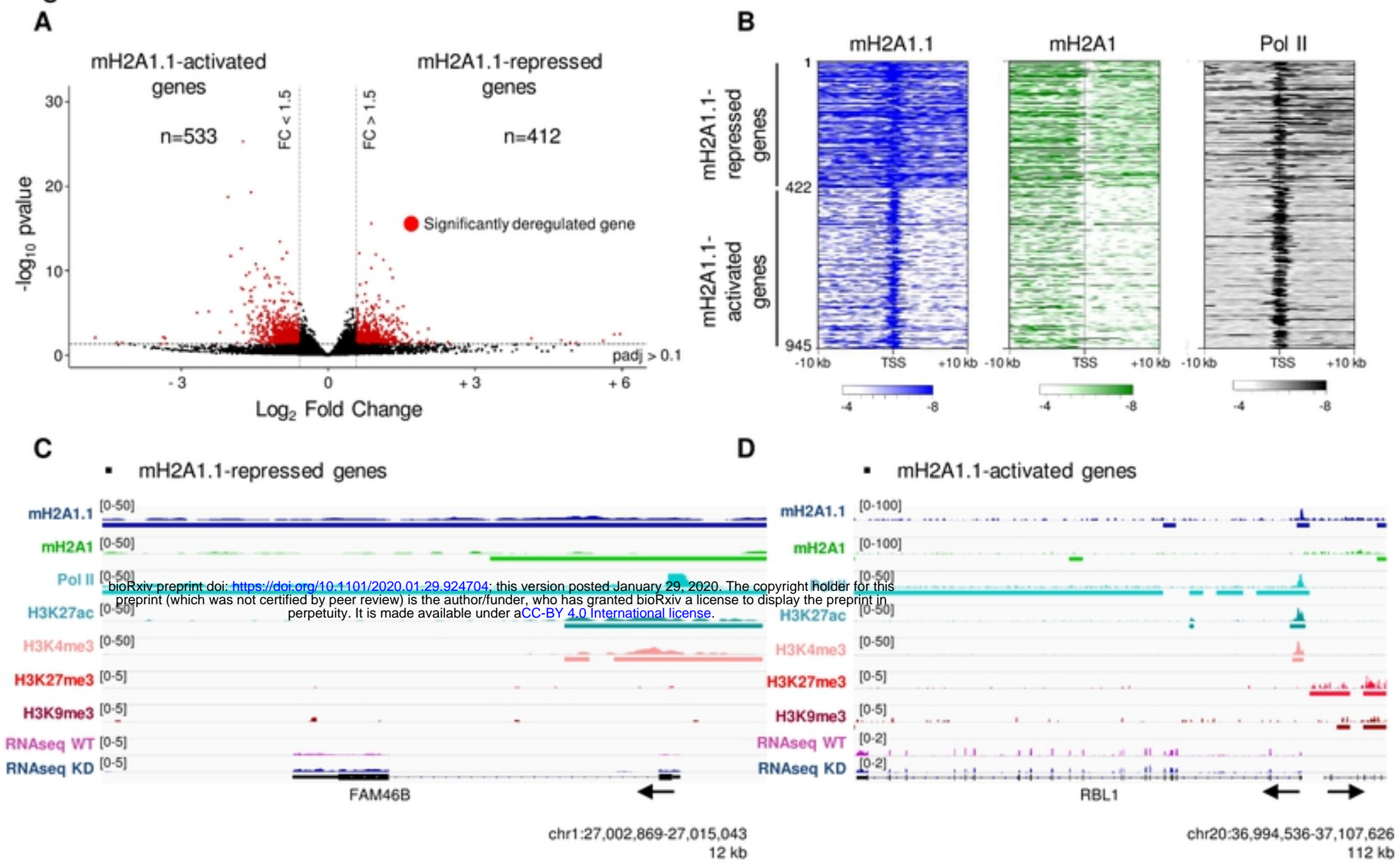


**E**

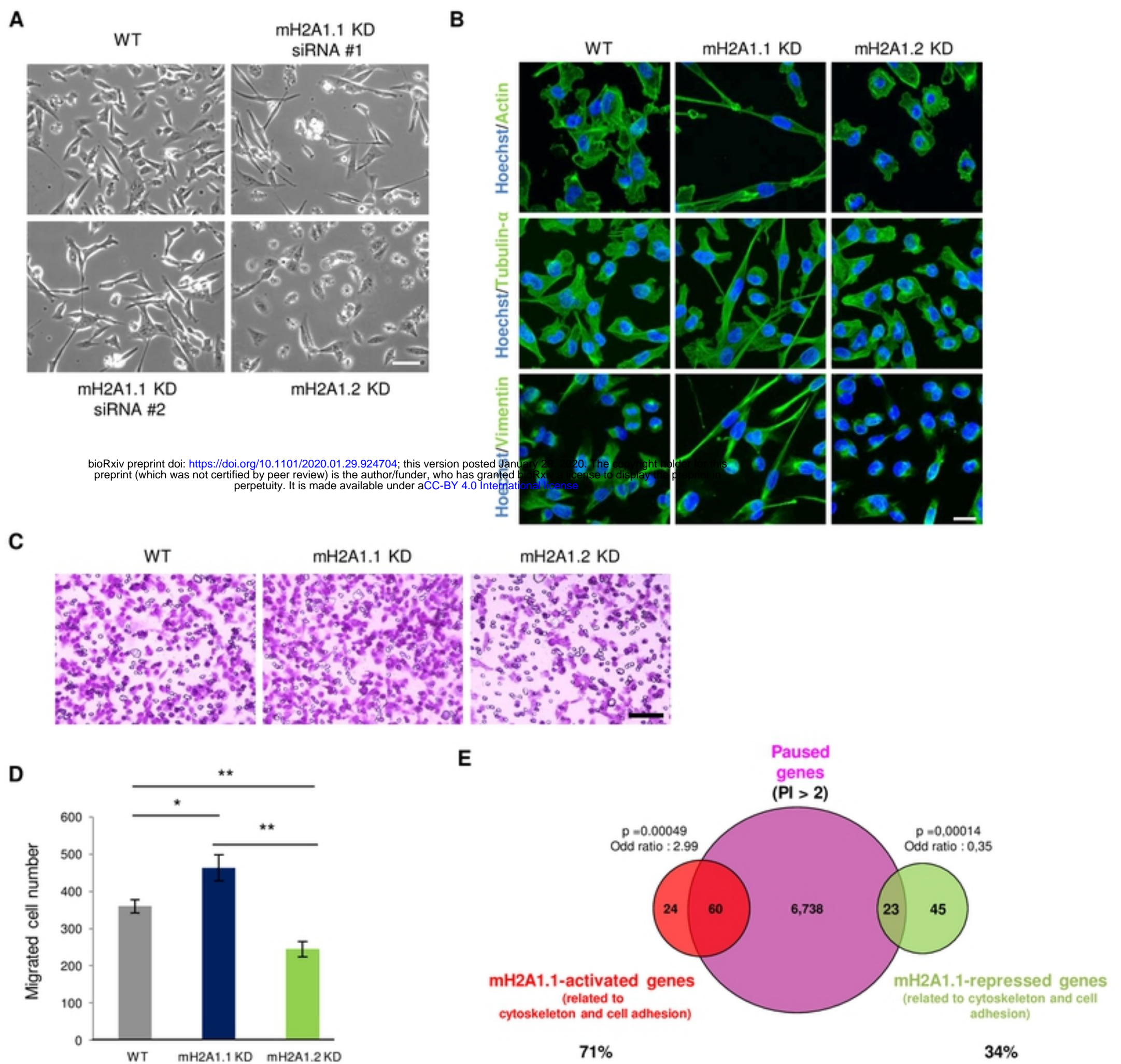


**F**

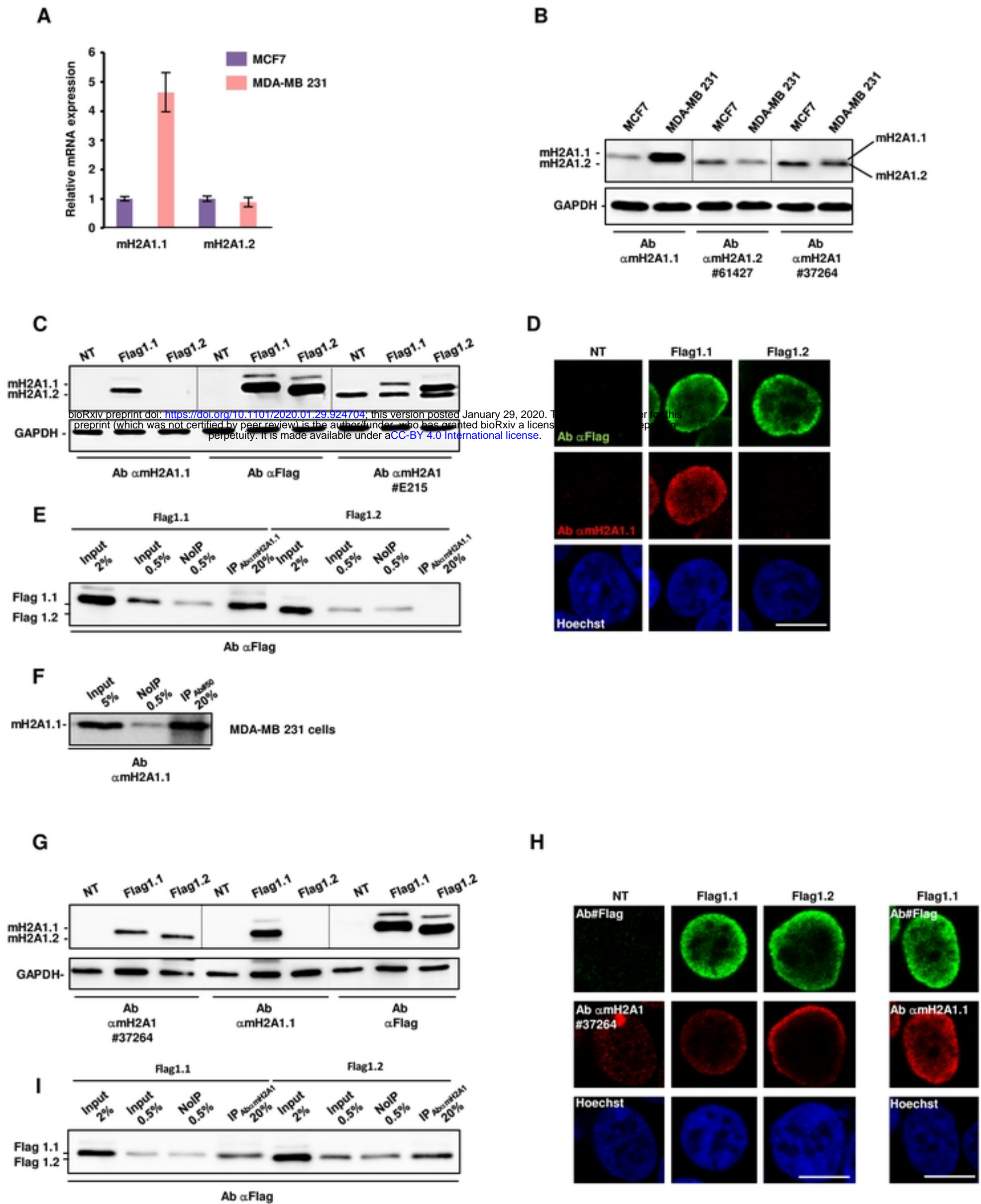


**Fig 4**

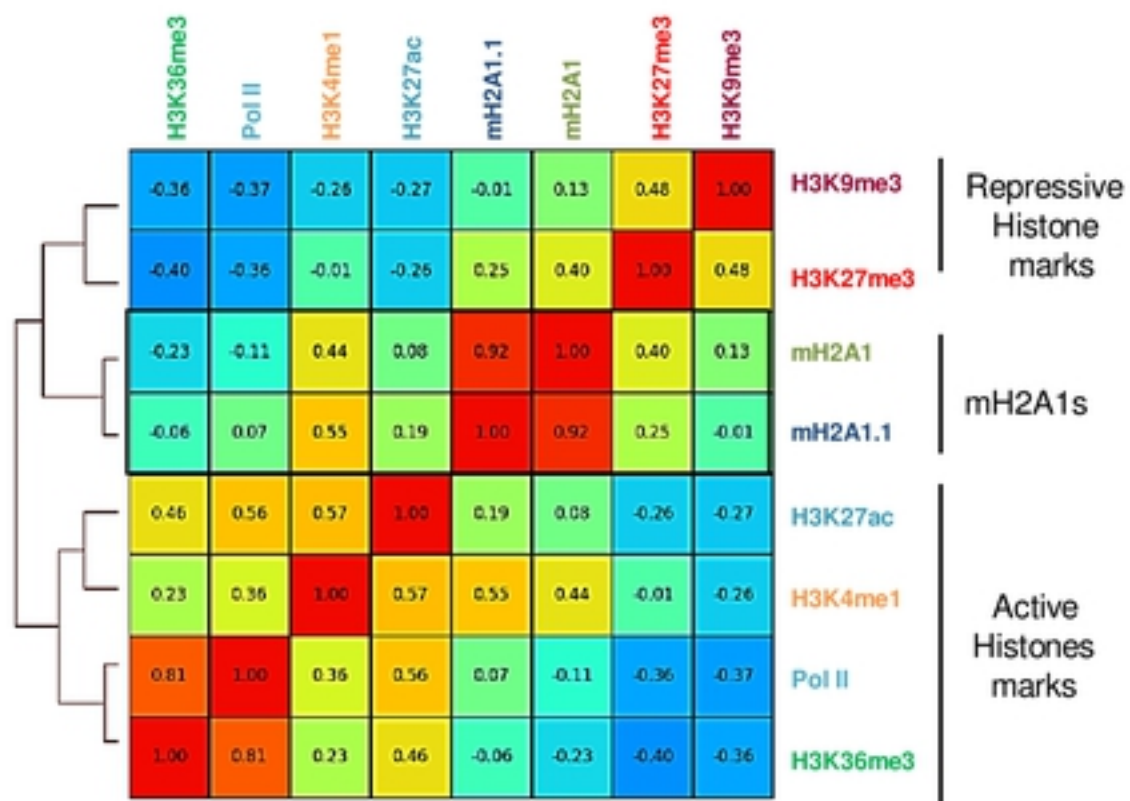


**Fig 6**

bioRxiv preprint doi: <https://doi.org/10.1101/2020.01.29.924704>; this version posted January 29, 2020. The copyright holder for this preprint (which was not certified by peer review) is the author/funder, who has granted bioRxiv a license to display the preprint in perpetuity. It is made available under aCC-BY 4.0 International license.



A

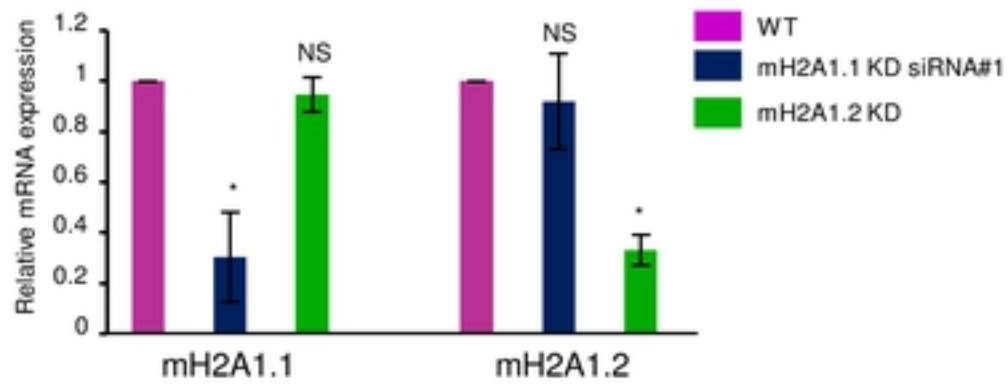


bioRxiv preprint doi: <https://doi.org/10.1101/2020.01.29.924704>; this version posted January 29, 2020. The copyright holder for this preprint (which was not certified by peer review) is the author/funder, who has granted bioRxiv a license to display the preprint in perpetuity. It is made available under aCC-BY 4.0 International license.

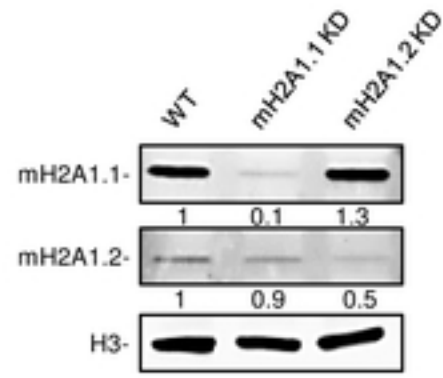
B

Genomic regions	PCC between mH2A1.1 and mH2A1
Heterochromatin	0.94
Enhancer	0.80
TSS +/- 1kb	0.41
TSS	-0.07

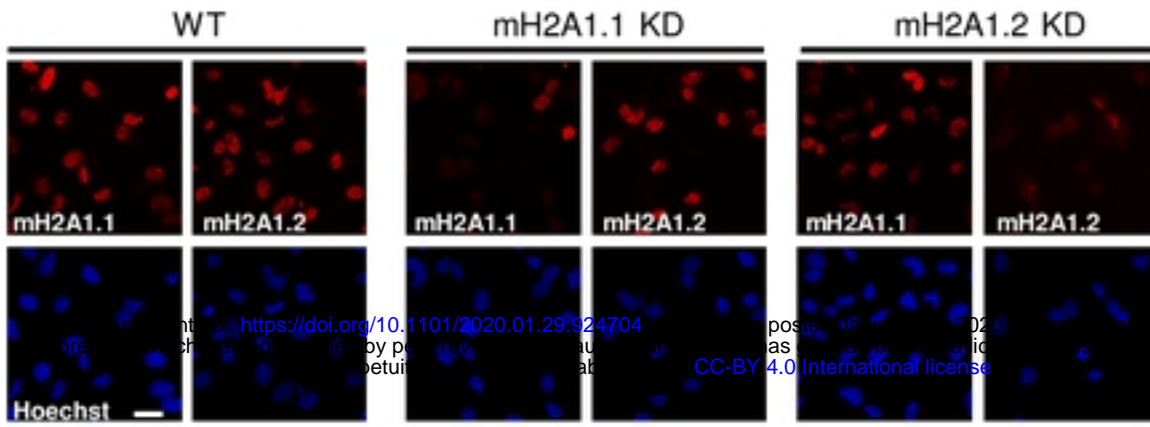
**A**



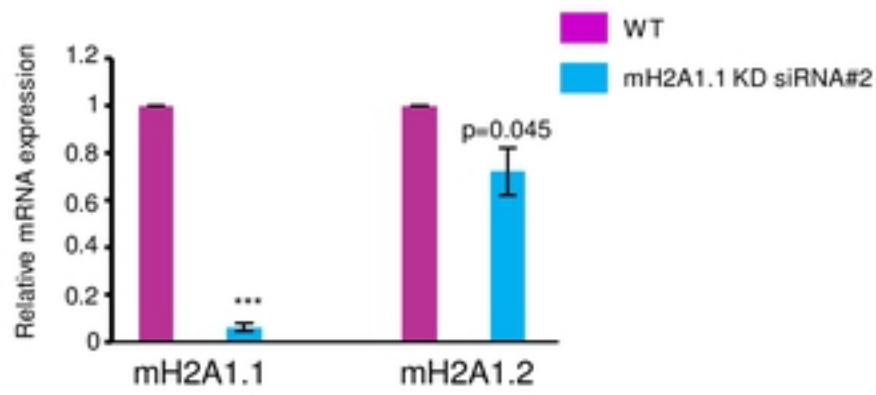
**B**



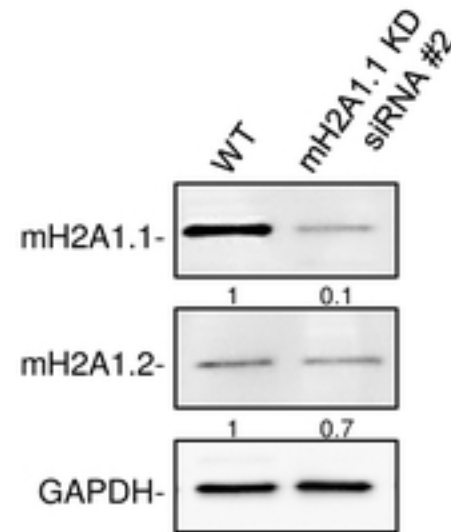
**C**



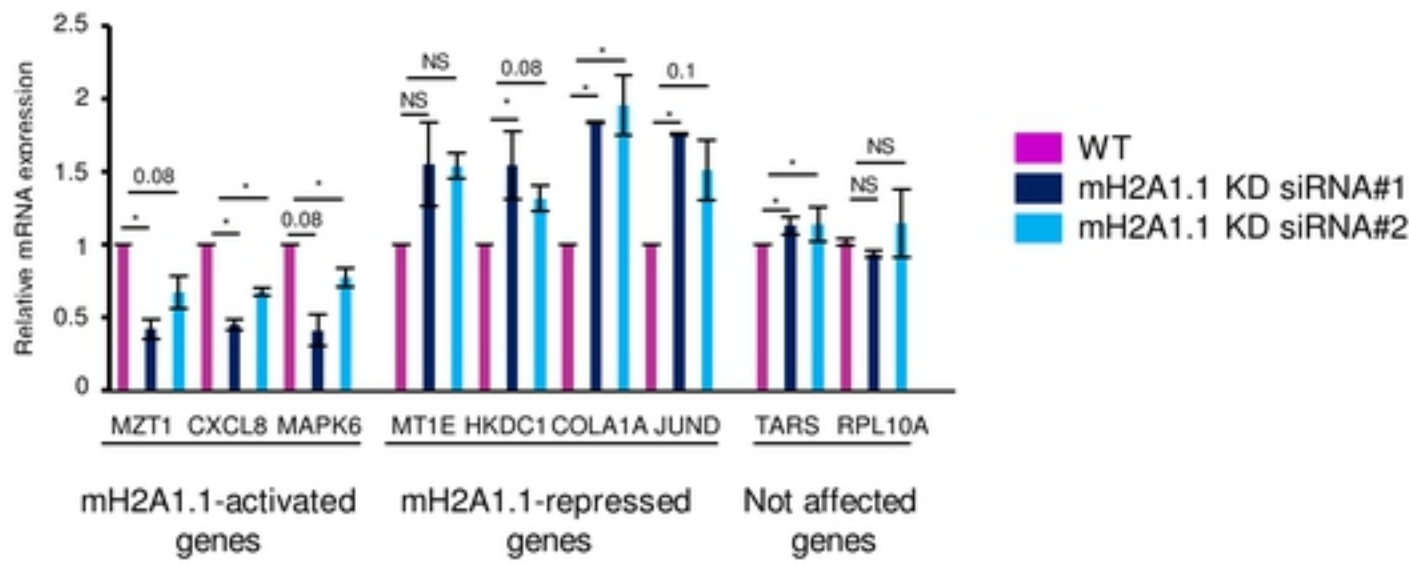
**D**



**E**

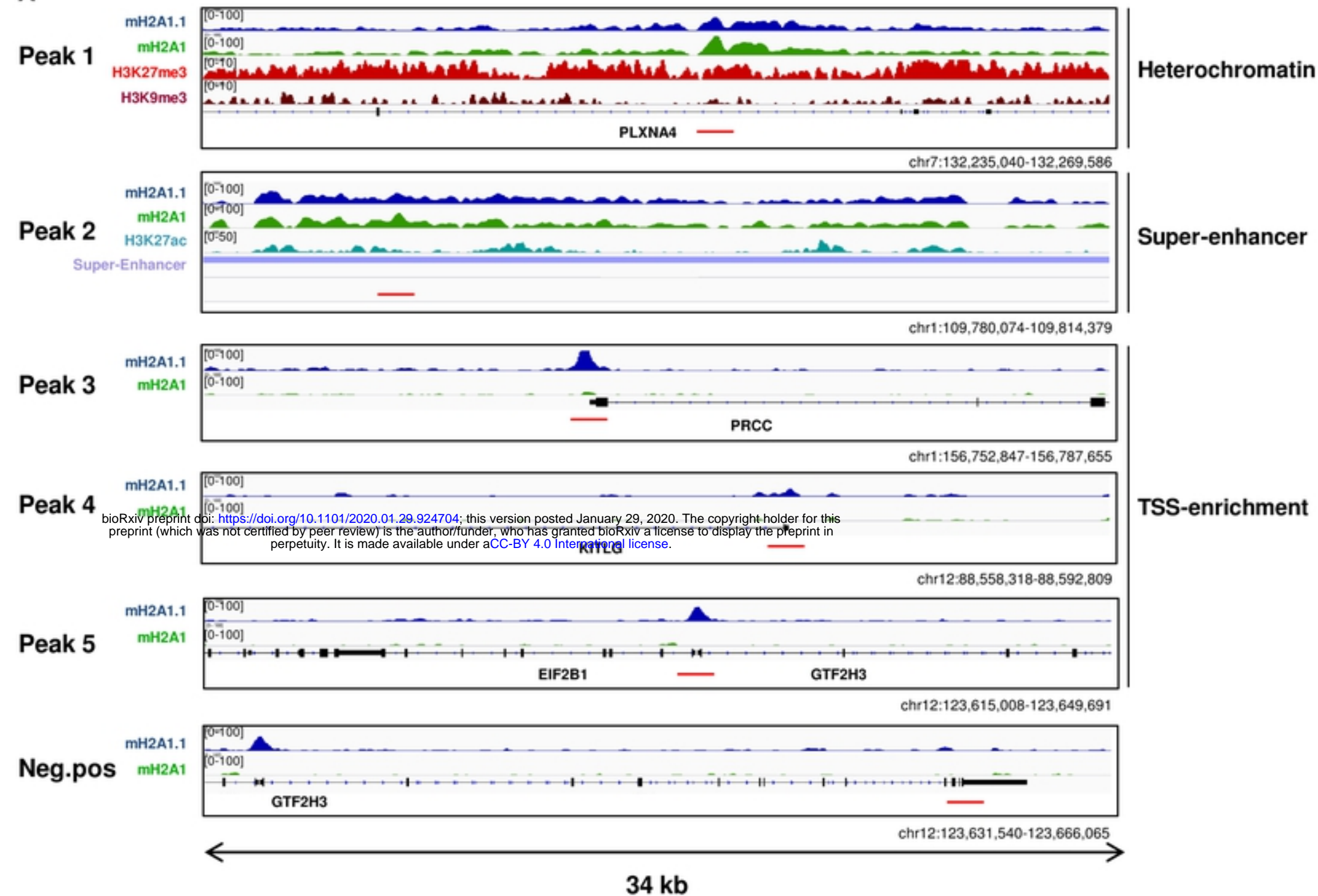


**F**



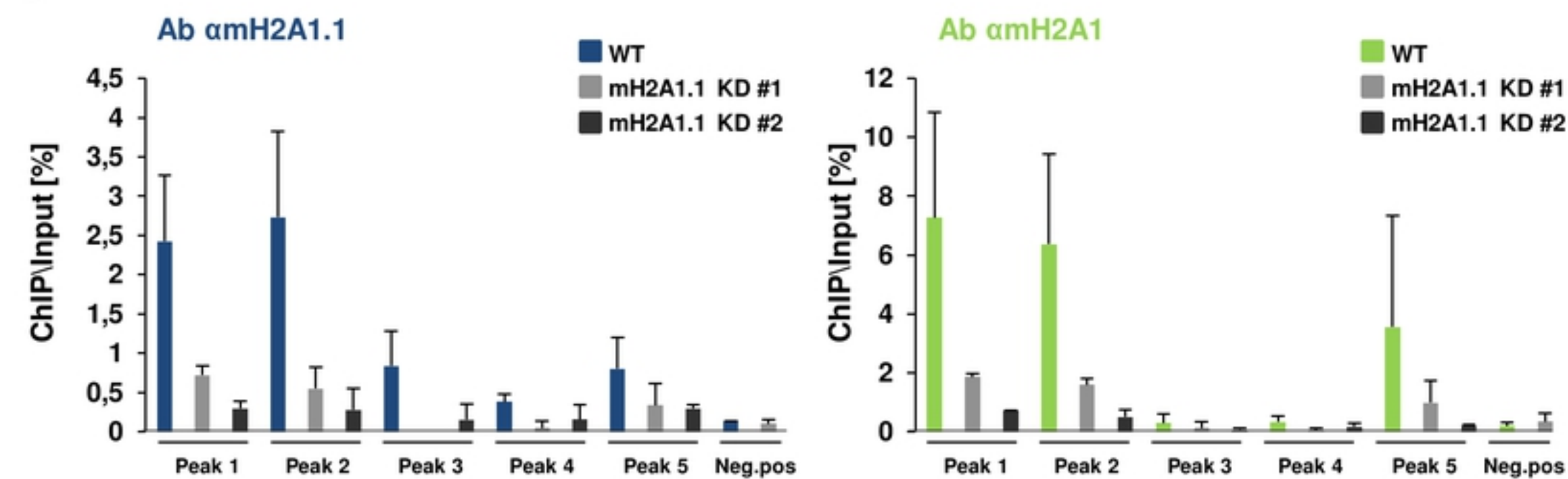
S4\_Fig

A

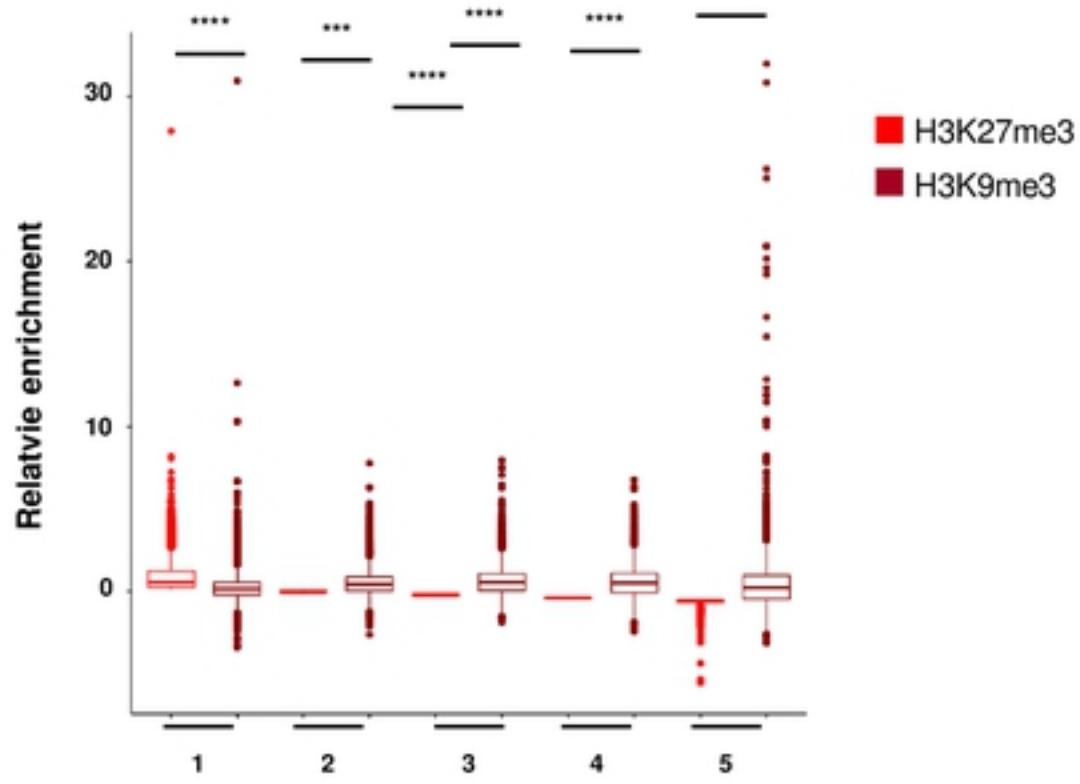


bioRxiv preprint doi: <https://doi.org/10.1101/2020.01.29.924704>; this version posted January 29, 2020. The copyright holder for this preprint (which was not certified by peer review) is the author/funder, who has granted bioRxiv a license to display the preprint in perpetuity. It is made available under aCC-BY 4.0 International license.

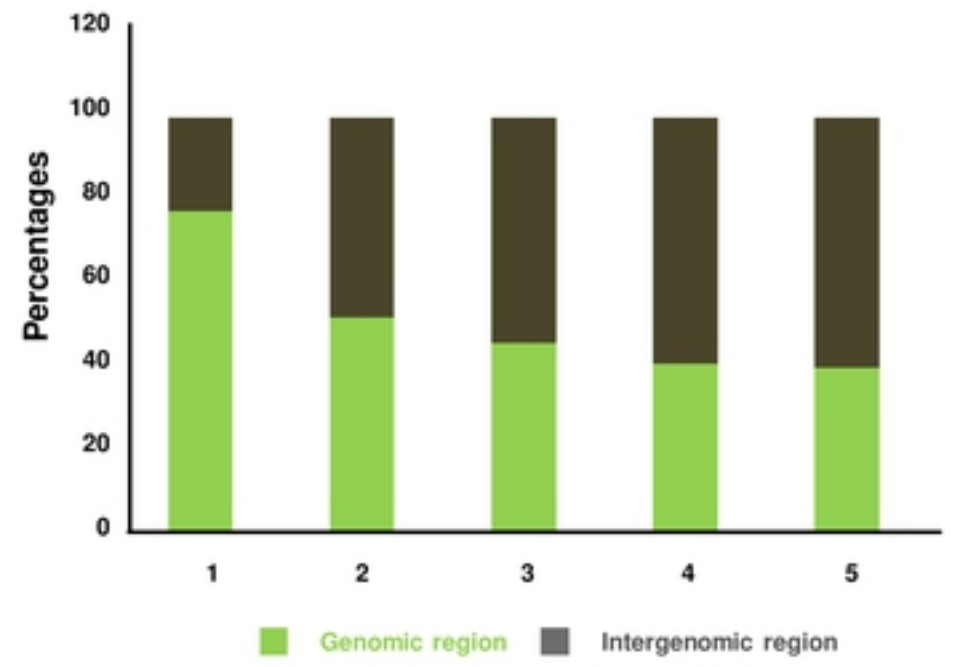
B



A



B



bioRxiv preprint doi: <https://doi.org/10.1101/2020.01.29.924704>; this version posted January 29, 2020. The copyright holder for this preprint (which was not certified by peer review) is the author/funder, who has granted bioRxiv a license to display the preprint in perpetuity. It is made available under aCC-BY 4.0 International license.

1 : Very high level of H3K27me3

2 : High level of H3K27me3

3 : Middle level of H3K27me3

4 : Low level of H3K27me3

5 : Very low level of H3K27me3

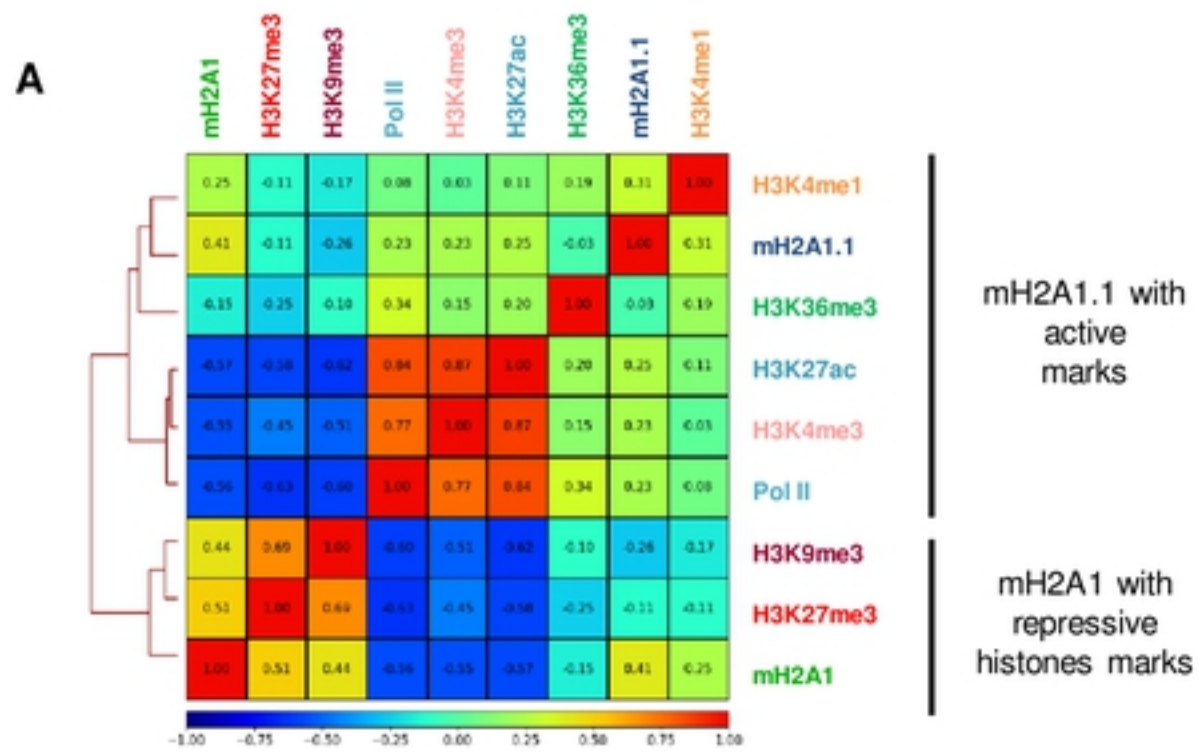
1 : Very high ratio of H3K27me3/H3K9me3

2 : High ratio of H3K27me3/H3K9me3

3 : Middle ratio of H3K27me3/H3K9me3

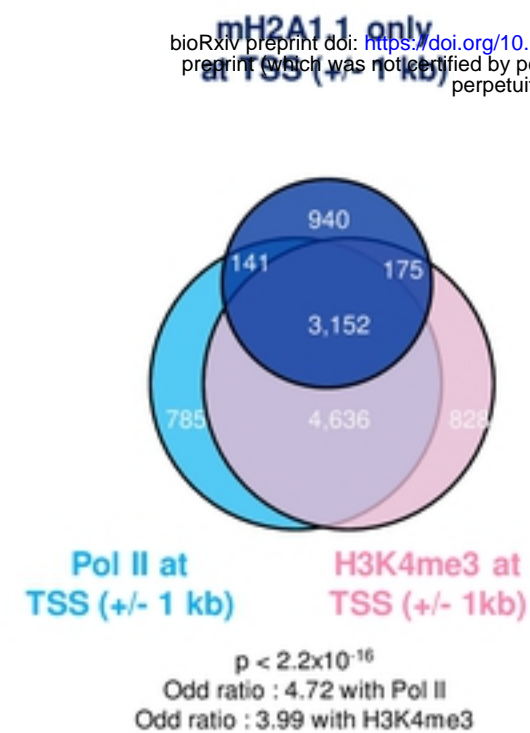
4 : Low ratio of H3K27me3/H3K9me3

5 : Very low ratio of H3K27me3/H3K9me3

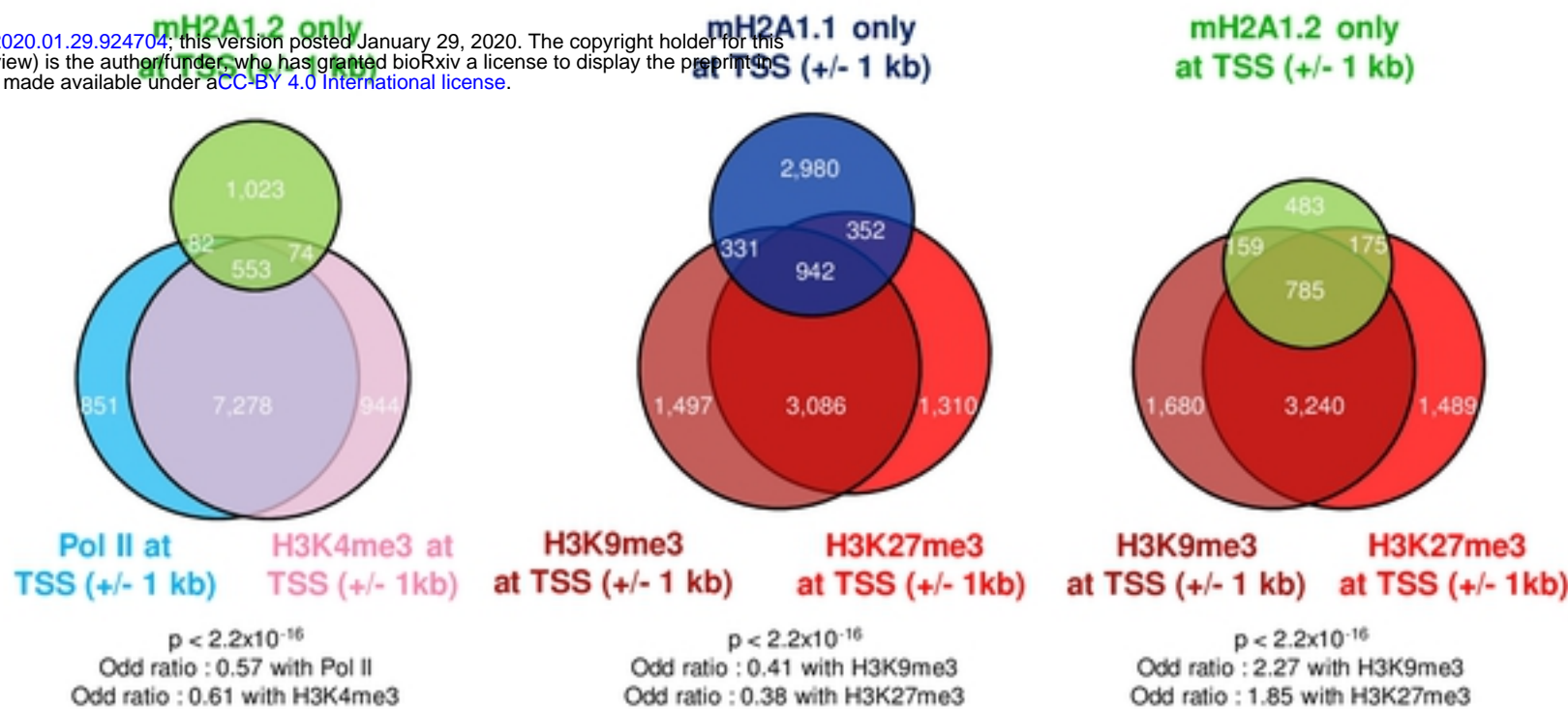


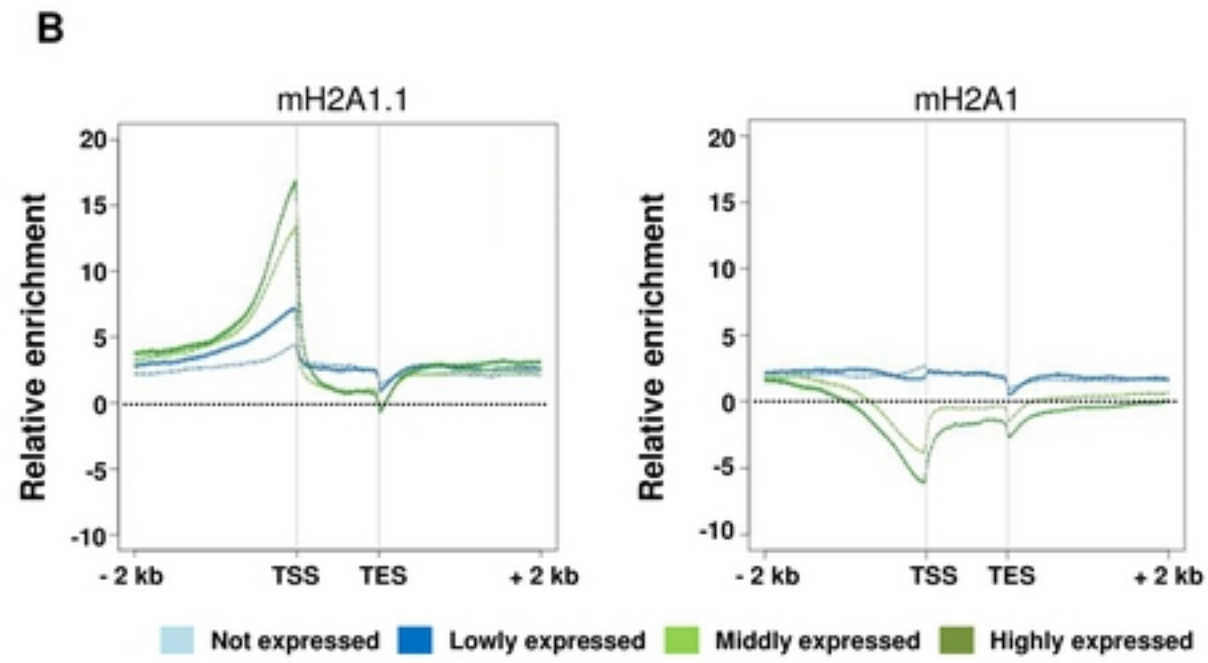
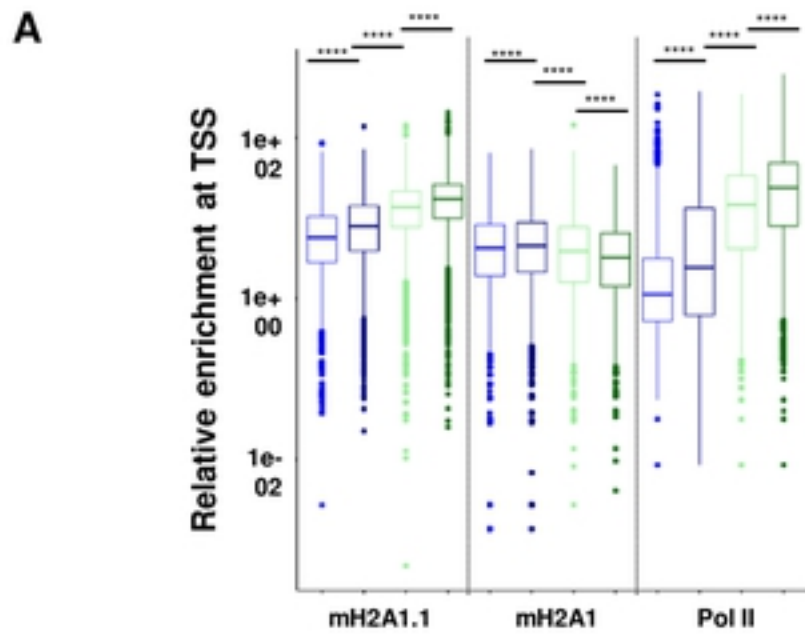
**B**

bioRxiv preprint doi: <https://doi.org/10.1101/2020.01.29.924704>; this version posted January 29, 2020. The copyright holder for this preprint (which was not certified by peer review) is the author/funder, who has granted bioRxiv a license to display the preprint in perpetuity. It is made available under aCC-BY 4.0 International license.



**C**

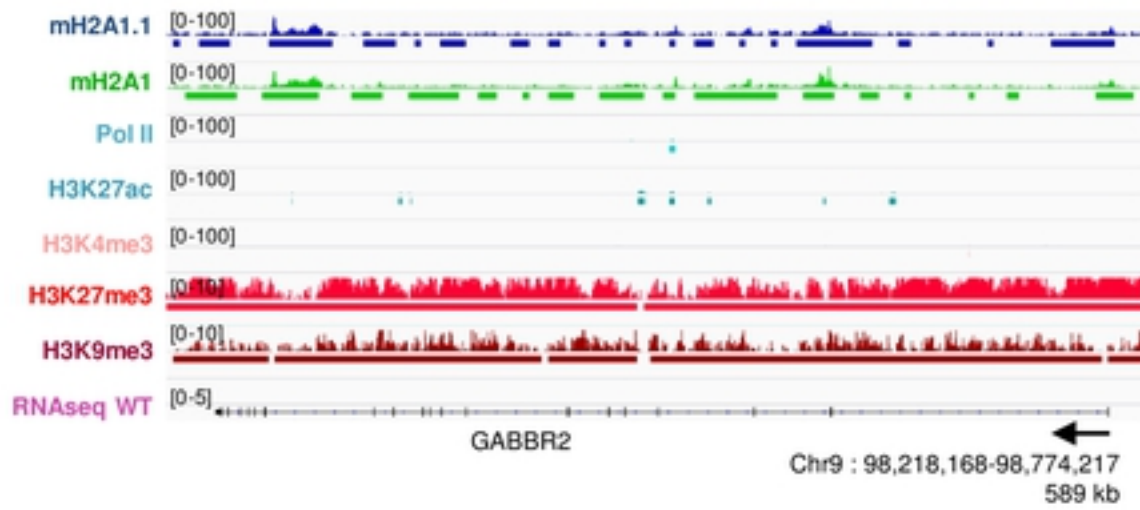




**C**

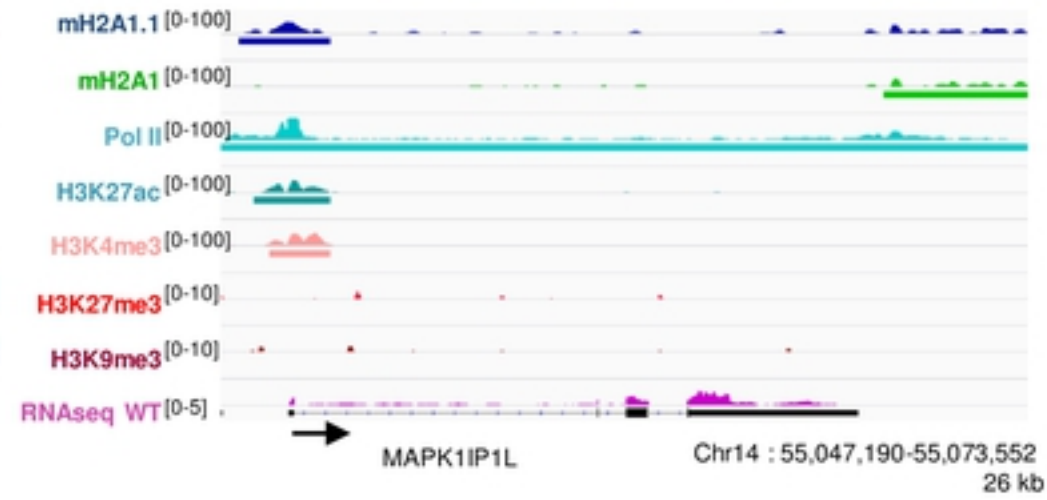
bioRxiv preprint doi: <https://doi.org/10.1101/2020.01.29.924704>; this version posted January 29, 2020. The copyright holder for this preprint (which was not certified by peer review) is the author/funder, who has granted bioRxiv a license to display the preprint in perpetuity. It is made available under aCC-BY 4.0 International license.

▪ Not expressed gene

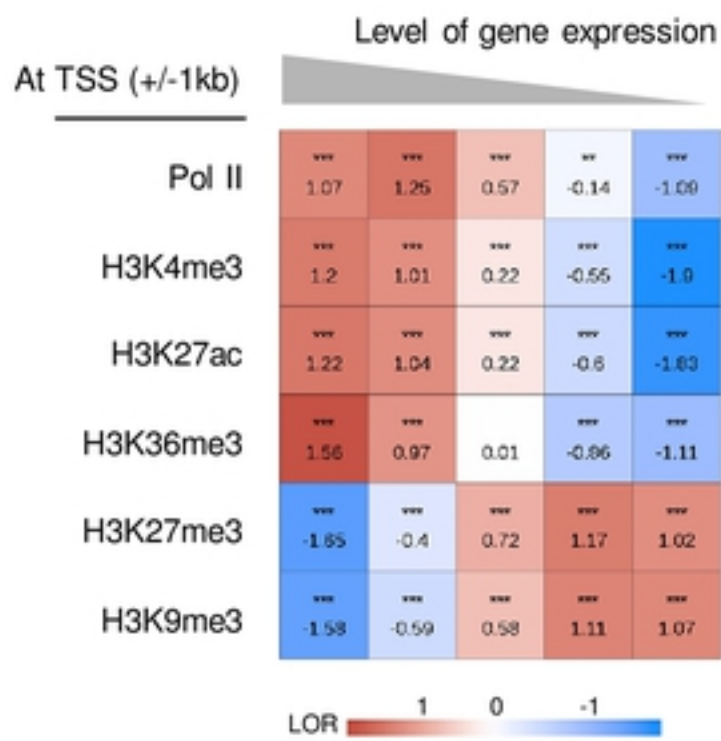


**D**

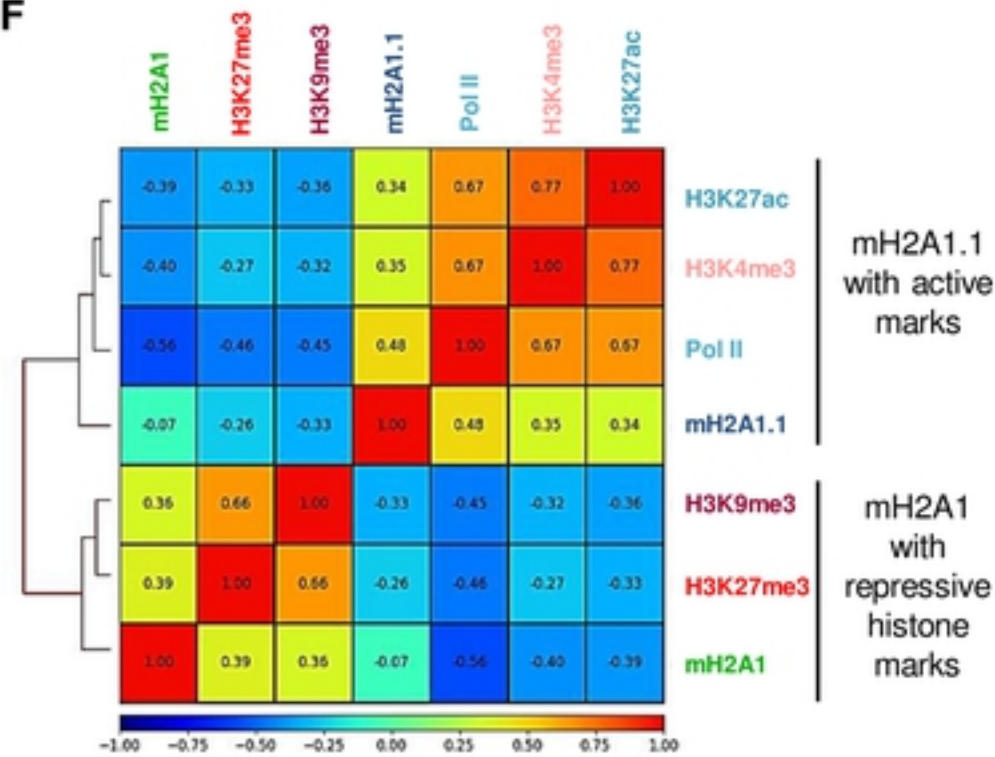
▪ Highly expressed gene



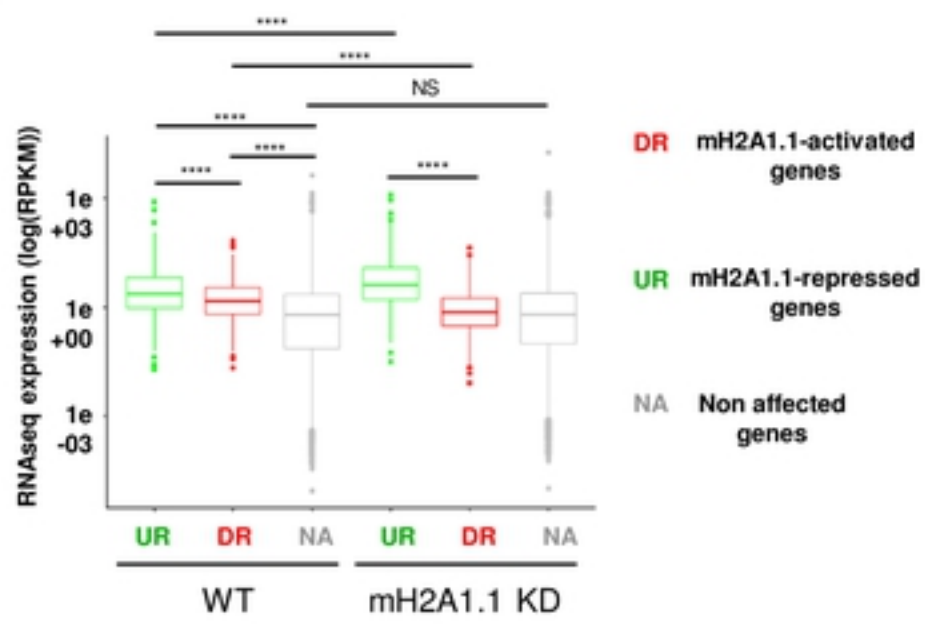
**E**



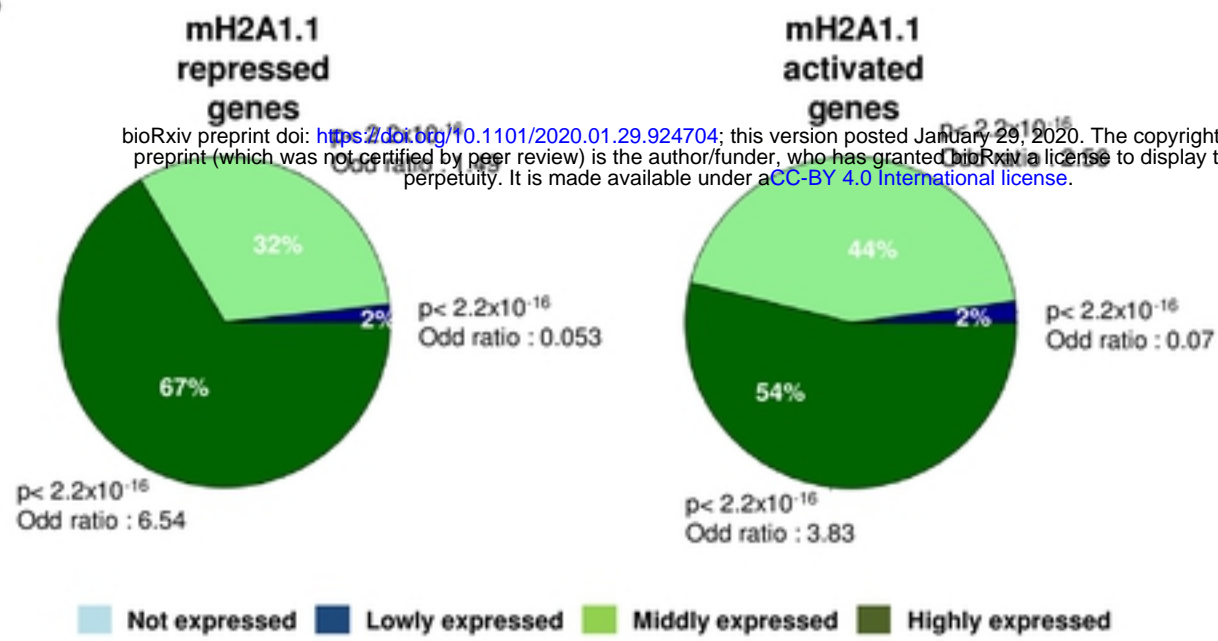
**F**



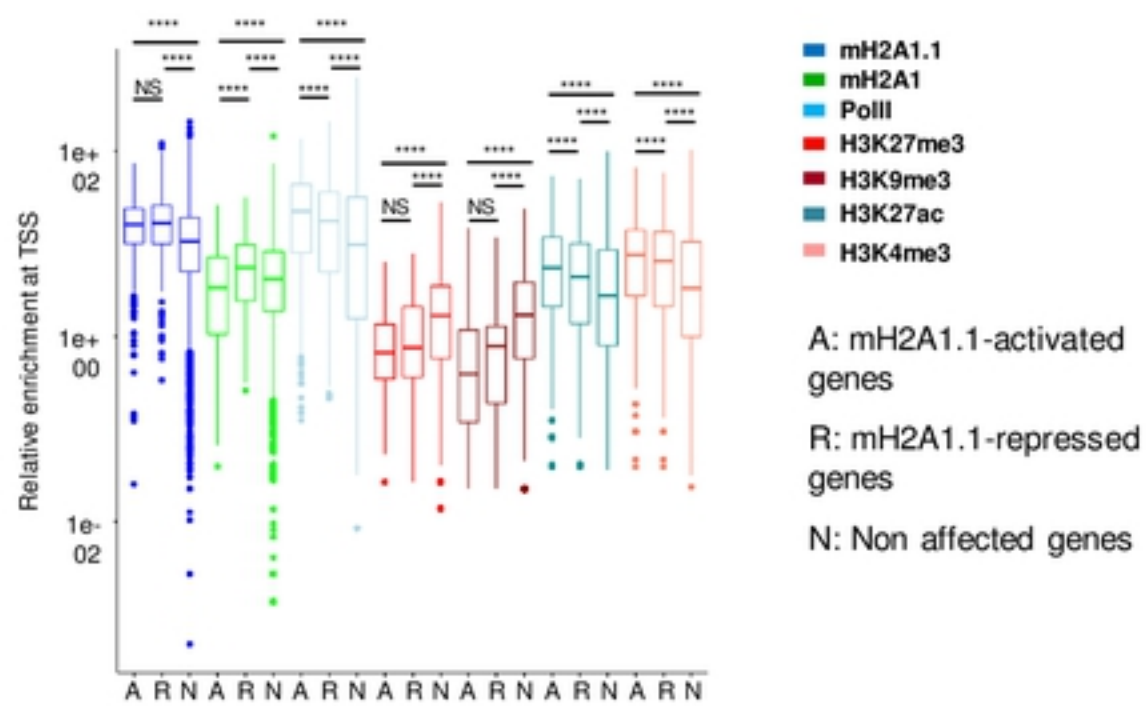
A



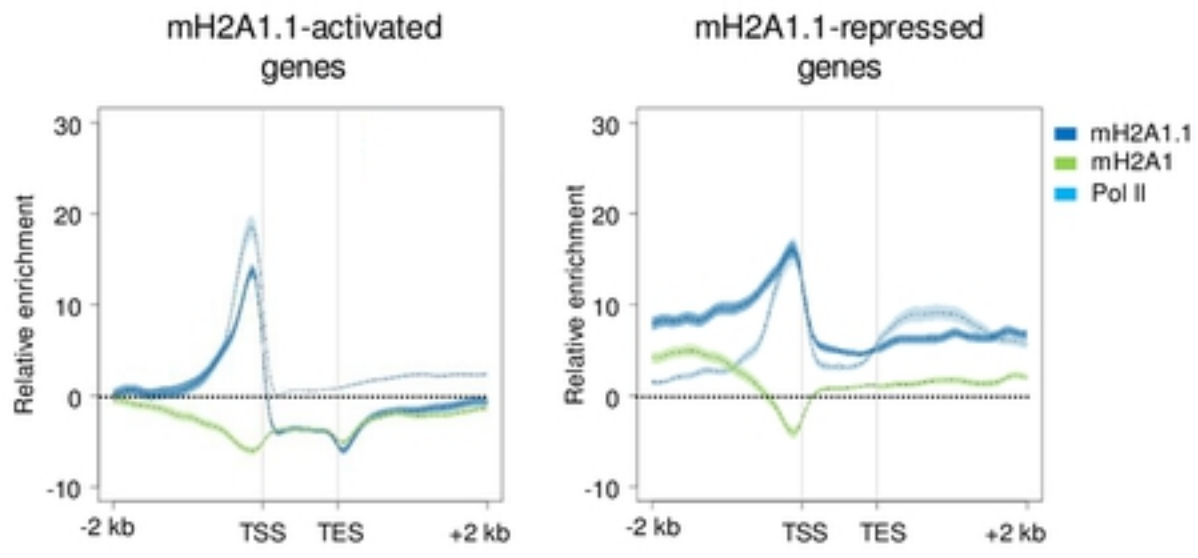
B



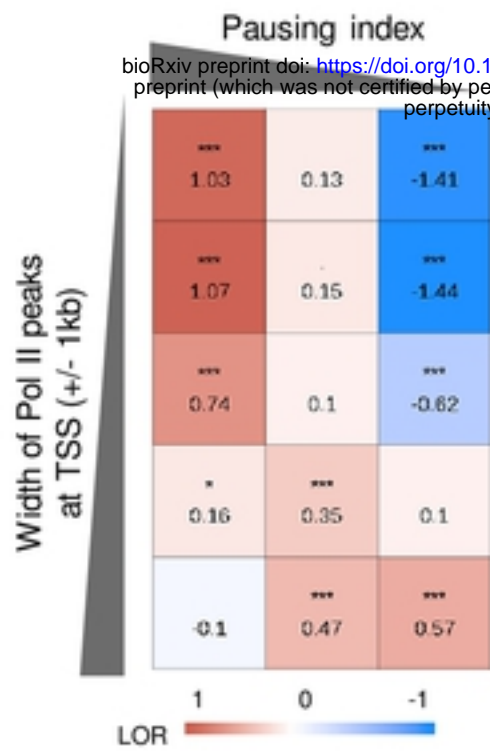
C



A



B



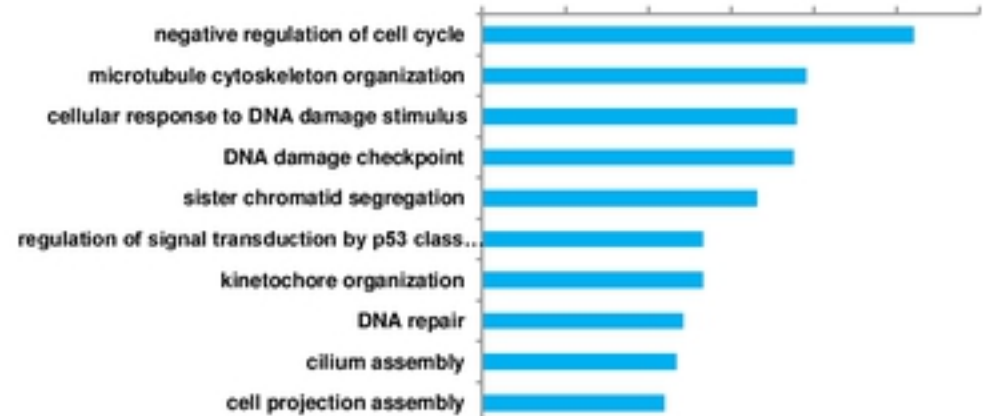
A

## mH2A1.1-activated genes

Biological process

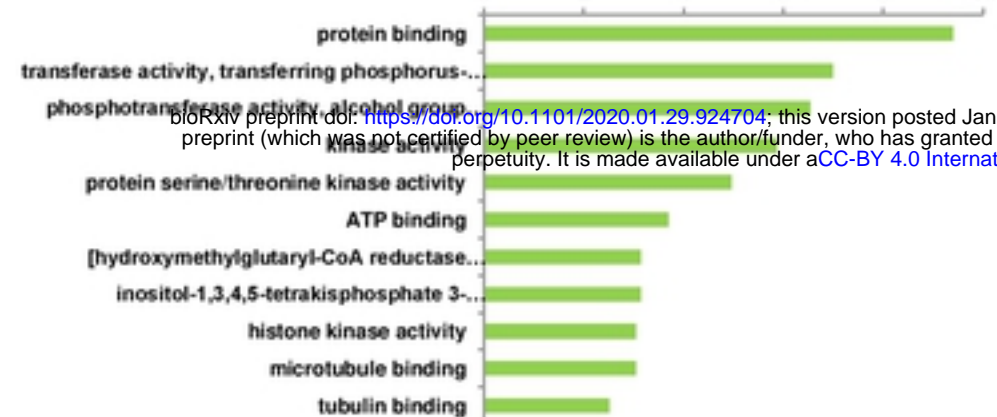
-log(pVal)

0 2 4 6 8 10 12



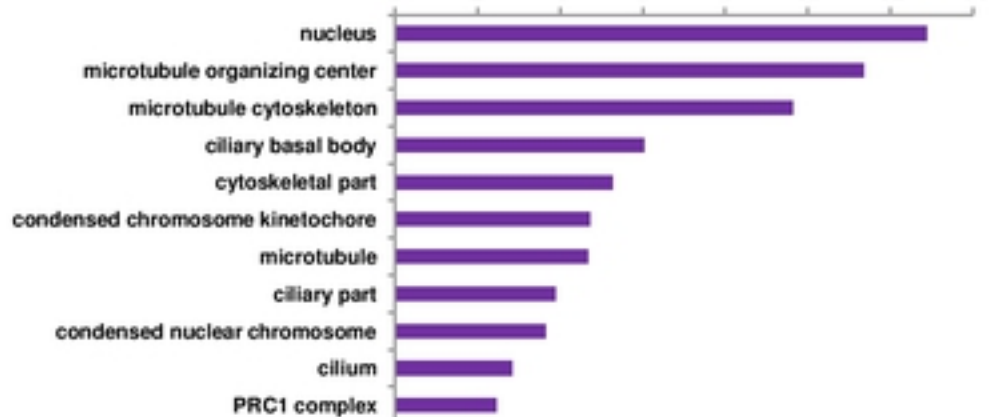
Molecular function

0 2 4 6 8 10



Cellular component

0 2 4 6 8 10 12 14



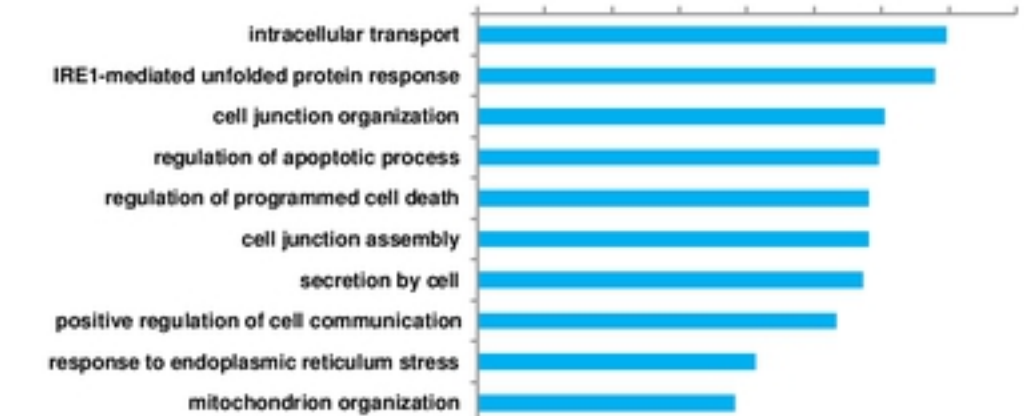
B

## mH2A1.1-repressed genes

Biological process

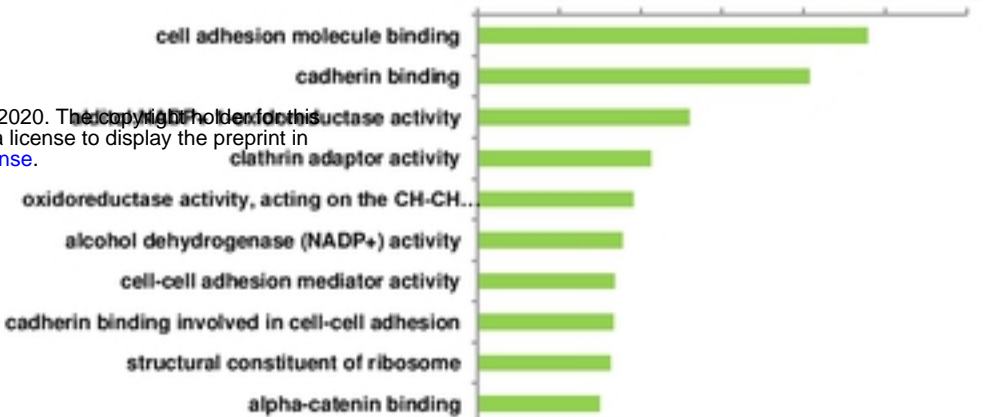
-log(pVal)

0 1 2 3 4 5 6 7 8



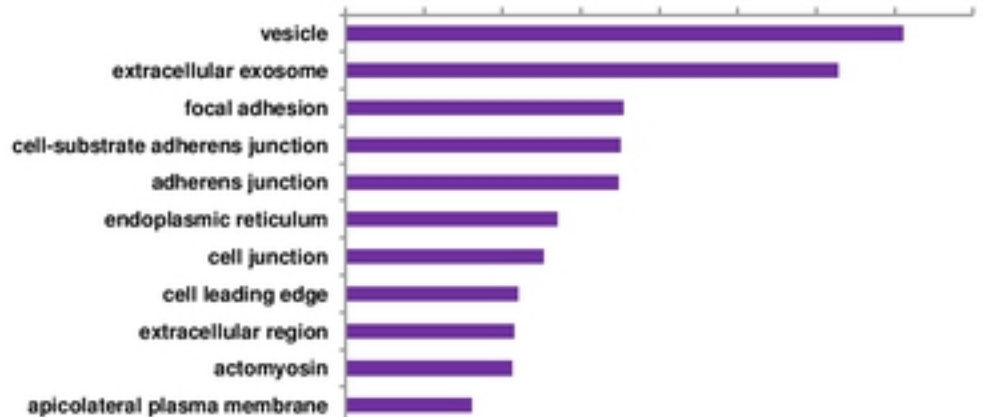
Molecular function

0 2 4 6 8 10 12



Cellular component

0 2 4 6 8 10 12 14 16



bioRxiv preprint doi: <https://doi.org/10.1101/2020.01.29.924704>; this version posted January 29, 2020. The copyright holder for this preprint (which was not certified by peer review) is the author/funder, who has granted bioRxiv a license to display the preprint in perpetuity. It is made available under aCC-BY 4.0 International license.